Title

PHOTODISSOCIATION OF NaI VAPOR AND THE ENERGY DEPENDENCE OF THE QUENCHING OF Na* (3p2p) BY FOREIGN GASES

Authors

Earl, Boyd L.
Herm, Ronald R.
Mims, Charles A.
et al.

Publication Date

1971-09-01

Submitted to Journal of
Chemical Physics

LBL-102
Preprint

PHOTODISSOCIATION OF NaI VAPOR AND THE ENERGY DEPENDENCE OF THE QUENCHING OF Na^* $(3p^2p)$ BY FOREIGN GASES

Boyd L. Earl, Ronald R. Herm,
Charles A. Mims, and Shen-Maw Lin

September 1971

AEC Contract No. W-7405-eng-48

DISCLAIMER

PHOTODISSOCIATION OF NaI VAPOR AND THE ENERGY DEPENDENCE OF THE QUENCHING OF Na^* ($3p\,^2P$) BY FOREIGN GASES

Boyd L. Earl, Ronald R. Herm[†], Charles A. Mims, and Shen-Maw Lin

Inorganic Materials Research Division,
Lawrence Berkeley Laboratory and
Department of Chemistry, University of California,
Berkeley, California 94720

ABSTRACT

Fluorescence of the Na^* ($3p\,^2P$) D-lines is observed upon photodissociation of NaI vapor by 1900-2500 Å radiation obtained through a monochromator from a high current, low pressure H_2 arc continuum source; the properties of this source are briefly described. The D-lines fluorescence efficiency exhibits a threshold at $\sim$ 2225 Å, and a relative minimum at $\sim$ 2500 Å, a relative maximum at $\sim$ 2050 Å. An expression is derived for the distribution in laboratory speeds of an atom produced by photodissociation of a diatomic molecule at thermal equilibrium. This expression is then employed to calculate the distributions in speeds of the photodissociatively generated Na^* and these

---

[†]Alfred P. Sloan Foundation Fellow.

computed Na^* speed distributions are employed to analyze the observed attenuations of the D-lines fluorescence upon addition of foreign gases. In this manner, the dependences on relative collision velocity g of the cross sections Q_q for collisional quenching of Na^* by CO_2, C_2H_4, CH_3CN, CF_3Cl, C_6H_6, SO_2, and I_2 have been determined. Over the range in g studied in this work ($\sim$ 1.0 - 2.5 km/sec), Q_q varies approximately as $g^{-4/s}$, with s in the range of 4-6, for all seven quenching gases. At a fixed value of g, Q_q varies as: $I_2 > SO_2 > C_6H_6 > CH_3CN > CF_3Cl > C_2H_4 > CO_2$. These results on the quenching cross sections are discussed in terms of the long-range forces between the reactants, including a possible long-range electron transfer curve crossing for the collision of Na^* with I_2 or SO_2. These measured quenching cross sections are also compared with previous literature values; good agreement is found in most cases, although some discrepancies are noted.

In 1926, Terenin[1] observed that the optical dissociation of NaI vapor produced electronically excited Na^* atoms. This was followed by the observation of the same phenomenon in the vapors of a number of diatomic halide molecules.[2] Soon after this discovery, it was realized that this phenomenon made possible measurements of the collisional quenching of electronic excitation of the atomic photodissociation product. When employed to measure collisional quenching cross sections, this method of photodissociative preparation of the electronically excited atom affords two advantages. Thus, it is possible to use as quenching gases species which would react with the ground state atom, but which are inert in the presence of the diatomic gas being photodissociated. It is this advantage of the method which made possible measurements[3,4] of thermally averaged cross sections for quenching of the $6^2P_{3/2}$ metastable state of Tl. Additionally, by varying the photodissociation wavelength, it is possible to vary the speed of the electronically excited atom produced. This has made possible measurements of the energy dependence of the cross sections for collisional quenching of the resonance radiation of sodium[5-12], potassium[13], and thallium[10,11,14-16] atoms.

Within the past decade, crossed molecular beam studies[17] of the reactions of ground state alkali atoms have supplemented the older diffusion flame data on alkali atom reaction kinetics and have

provided a good deal of insight into the reaction dynamics of ground state alkali atoms. This has led to a renewed interest in the collisional quenching of excited metal atoms. For example, Refs. 4 and 11 draw analogies between their results on quenching collisions and molecular beam results on analogous reactions of ground state species. In our own laboratory, this has prompted a program to measure the cross sections for quenching of excited alkali atoms. This present paper reports initial results of this program on the quenching of $3p\,^2P$ Na*, as well as a more detailed examination of this particular experimental technique for measuring the energy dependence of quenching cross sections.

EXPERIMENTAL CONDITIONS

The apparatus employed in this study was similar to that described in Ref. 9. Continuous radiation, of constant intensity, from a source described below was focused through a Heath Model EU-700 monochromator: f/6.8 at 2000 Å with a reciprocal dispersion of approximately 20 Å/mm at the exit slit. The ultraviolet radiation exiting from the monochromator was chopped at $\sim$ 80Hz and focused into a heated quartz cell containing the NaI vapor. Except where noted, the monochromator was operated with 2 mm slits. This provided radiation centered about the nominal wavelength setting with an approximately triangular distribution function characterized by a 47 Å FWHM bandspread, or an energy spread of $\sim$ 950 cm^{-1} at 2250 Å; the experimental consequences of the monochromator bandwidth are discussed later and shown to be minor. Upon exiting from the sample cell, the ultraviolet radiation

impinged upon an RCA 1P21 photomultiplier tube which had been sprayed with a coating of sodium salicylate. Since the fluorescence efficiency of sodium salicylate is reported[18] to be constant for the wavelength region studied here, the output signal from this phototube was proportional to the flux of incident ultraviolet photons. The sodium fluorescence intensity produced by photodissociation of the NaI vapor in the cell was observed at a right angle to the ultraviolet flux through a Baird Atomic B-11 interference filter; this filter, with a transmission bandwidth of ∿ 15 Å FWHM, isolated the 5896 and 5890 Å sodium D-lines. The D-lines fluorescence transmitted through the filter was detected by an RCA 7265 photomultiplier and measured by a PAR HR-8 amplifier locked-in on the ∿ 80Hz oscillation imposed on the ultraviolet radiation.

The vapor cell was constructed from 30 mm quartz tubing, ∿ 16.5 cm in height. Four flat windows, two of suprasil for the ultraviolet beam and two of quartz, were equally spaced at 90° about the tube circumference, ∿ 4 cm down from the top. Each window extended out ∿ 1.25 cm from the tube wall, so that the optical path of the ultraviolet through the cell was ∿ 5.5 cm. At its top, the 30 mm quartz tube was connected to the vacuum line through a 3 mm i.d. opening which could be sealed by a magnetically operated ground quartz rod. The 30 mm tube was joined at the bottom to a 10 cm length of 10 mm quartz tubing which was charged with reagent grade NaI. This entire assembly was placed in a wire wound oven which contained viewing ports coinciding with the

windows in the cell. In order to prevent radiative cooling of these windows, they were further surrounded by additional heating coils. Two thermocouples were placed on the outside wall of the vapor cell, one just below the level of the windows and the other at the level of the charge of NaI salt. In operation, the temperature of the cell at the level of the windows was typically maintained 20-30°C hotter than that of the NaI charge, permitting independent variation of the temperature and pressure of the NaI vapor. The NaI vapor temperatures quoted in this paper refer to the temperature at the cell windows.

In the measurements of the collisional quenching of Na^*, the NaI in the cell was maintained at the temperature of the experiment for a few hours, with periodic exposures to the vacuum line. Following this degassing procedure, the foreign quenching gas was admitted to the cell by means of the ground quartz seal. The pressure of the quenching gas admitted was measured by means of a Texas Instruments spiral quartz manometer situated on the external gas line. Because the mean free path within the gas at the pressures of quenching gas employed here was much smaller than the diameter of the interconnecting tubing, the pressure of the quenching gas measured at room temperature on the external gas line was equated with the pressure of quenching gas inside the cell (Ref. 4 discusses this thermal transpiration correction).

All chemicals employed as quenching gases were purchased commercially (reagent grade where available) and used without further purification. In so far as all of these gases exhibited

relatively large quenching cross sections, the effects of small impurities should be negligible. It was also necessary to insure that the gases studied as quenching agents neither decomposed nor reacted with the NaI in the high temperature cell. Three experimental checks were employed to attempt to insure these conditions. As a first check, the behavior of the sodium fluorescence intensity upon admission of the foreign gas was examined. This resulted in the rejection of quite a few gases as possible quenching agents. Thus, the Na^* fluorescence was virtually extinguished upon admission of CCl_4 gas and failed to reappear upon evacuation of the cell. Similarily, BF_3 and NO_2 were rejected because admission of these gases to the cell produced a rapid drop in the Na^* fluorescence followed by a slower rise, suggestive of a slow chemical decomposition of these species. Admission of SF_6 to the cell at very low pressures ($\sim$ 0.1 Torr) resulted in very large and non-reproducible attenuations of the Na^* fluorescence. Trifluoromethane failed to quench the Na^* fluorescence, even at pressures as high as 50 Torr. Indeed, this gas had the opposite effect of enhancing the Na^* fluorescence by 20-30%, although the enhancement deteriorated with time. Related enhancement effects have been reported for thallium fluorescence[2] by NH_3 and sodium fluorescence[9] by H_2 at low pressures. As a second check, the constancy of the pressure of quenching gas was monitored while it was in the cell. This led to the rejection of propene, butene-1, butene-2, and toluene as possible quenching agents for study because, upon admission

of any of these gas to the hot cell, the pressure measured on the external gas line increased slowly, suggesting decomposition of the gas admitted into smaller molecular weight products.

The seven gases employed as quenching agents in this study (C_2H_4, CH_3CN, CF_3Cl, C_6H_6, SO_2, I_2, and CO_2) satisfied both of these checks. As a final check, samples of each of the first five gases listed were collected from the hot vapor cell after actual quenching experiments. The mass spectral patterns of these gas samples were identical (to within experimental accuracy) to those of samples of the same gases taken prior to exposure to the hot vapor cell. The quenching of Na^* fluorescence by CF_4, CH_4, and C_2H_6 was also examined briefly. These gases appeared to be stable in the hot NaI cell, but proved to have very small quenching cross sections (estimated as less than ~ 5 $Å^2$).

Another effect which could invalidate the measured quenching cross sections arises when the foreign gas admitted to the cell absorbs a fraction of the ultraviolet being used to photodissociate the NaI. In such a case, the attenuation of the steady-state Na^* fluorescence is due to a combination of the collisional quenching of the Na^* and of absorption of the ultraviolet by the foreign gas. Of the seven quenching gases employed in this study, SO_2 and C_6H_6 absorbed[19] over a region of the NaI absorption continuum of interest. The ultraviolet absorptions by these gases were measured directly during the quenching experiments, and the quenching cross sections reported for SO_2 and C_6H_6 have been corrected for this effect. Another gas, CS_2, was studied briefly, but proved to absorb too strongly to permit quenching studies.

The Hydrogen Arc Ultraviolet Continuum Source

Initially, a high pressure Xe-Hg arc was employed as the source of the continuum ultraviolet radiation. However, this source was abandoned in favor of a low pressure H_2 arc patterned after a description due to Finkelstein[20] because the high output of visible radiation from the Xe-Hg arc proved troublesome. A brief description of this H_2 arc is given here because some initial difficulty was encountered in obtaining reliable operation. These remarks are intended to complement Finkelstein's[20] description. Figure 1 presents a schematic diagram of the electrodes inside the water-cooled brass lamp housing together with the electronics necessary for DC operation. In striking the arc, the cathode is resistance heated and the starting electrode is connected to a tesla coil. A voltage of about 260 volts between anode and cathode is required to strike the arc with 6 Torr of H_2. The lamp has been operated with both DC and rectified AC; operation in the DC mode enhances stability. The arc provides a usable continuum from $\sim$ 1900 Å (the shorted wavelength examined) to above 3000 Å. Indeed, it provides an ultraviolet intensity through the monochromator and into the NaI cell which exceeds that provided by a Hanovia 1 kw high pressure Xe arc over the full 2000-3000 Å range and by a Hanovia 1 kw high pressure Xe - Hg arc below 2275 Å.

The nickel screen substrate cathode described in Ref. 20 is reinforced with a strip of tantalum foil down the middle, coated with a lacquer of barium-strontium carbonate, and folded into an accordian shape. Initially, the arc was difficult to strike and

the cathodes exhibited short lifetimes until it was realized that the method of preparation and activation of the cathode surface is critical. By depositing a barium-strontium oxide solid solution onto the nickel screen substrate according to the directions given in Ref. 21, cathodes were subsequently obtained which exhibit acceptable lifetimes (40-50 hours) and render the arc easy to strike and stable once struck.

Figure 2 shows the voltage-current-pressure-intensity relationship of the arc. The data are limited to arc voltages less than $\sim$ 120 V because the arc is unstable at higher voltages. Data are not given for arc currents higher than $\sim$ 16 A because of limitation of the DC power supply used. Typical operating conditions in these experiments were in the 12-15 A, 6-8 Torr of H_2 range.

PHOTODISSOCIATION OF NaI

The D-lines Fluorescence Efficiency

Figure 3 shows the observed dependence of the reduced fluorescence efficiency $R(\lambda_o)$ (defined as the ratio of the total number of D-lines photons detected per second to the number of ultraviolet photons per second incident on the NaI vapor) on the nominal wavelength λ_o of the ultraviolet impinging on the NaI vapor. In collecting this data, a temperature difference of $\sim$ 100°C was maintained between the lower part of the NaI cell, where the solid NaI sample resided, and the upper part of the cell where the NaI vapor was photo-dissociated. This had the effect of rendering the temperature

of the NaI vapor being photodissociated somewhat uncertain; for purposes of calculation, the temperature of the vapor was taken as the temperature at the windows of the cell. Since the vapor pressure of the NaI was governed by the lower temperature, however, the total absorption cross sections for NaI vapor quoted in Ref. 22 indicate that this procedure insured that the ultraviolet radiation was negligibly absorbed upon traversing the cell. It is probably worth emphasizing again that this temperature differential within the cell was maintained at $\sim$ 20° - 30°C in measurements of quenching cross sections, thereby reducing the uncertainties in the quoted gas temperatures in these experiments. Figure 3 indicates that the reduced efficiency curves are similar for all three temperatures studied, although extending to somewhat longer wavelengths at higher temperatures. The second region of fluorescence excitation by radiation below 2000 Å has not apparently been previously reported.[9,22]

In agreement with previous workers[1,9,11], the fluorescence peak at longer wavelengths shown in Fig. 3 is assigned to a transition of NaI from its ground state potential curve to the repulsive part of an excited state curve which dissociates into an excited Na atom (Na^*) and a ground state iodine atom, i.e.

$$NaI\ (X\ ^1\Sigma^+) \xrightarrow{\sim 2000 - \sim 2500 Å} Na^*\ (3p\ ^2P) + I\ (^2P_{3/2}). \quad (1)$$

A recent study[23] of the Doppler widths of the D-lines suggested that the photodissociation of NaI vapor at wavelengths longer than $\sim$ 2100 Å might not proceed exclusively by excitation of NaI

to a repulsive state which dissociated into Na^* and I within one vibrational period. However, the more recent study by Brus[11] of the Na^* fluorescence lifetime indicated that the fluorescence is indeed a consequence of the direct photodissociative process depicted in Eq. (1).

The origin of the second, shorter wavelength fluorescence region shown in Fig. 3 is uncertain. It might be due to either or both of the following direct photodissociative processes:

$$NaI\ (X\ ^1\Sigma^+) \xrightarrow{?\ -\ 2100\text{Å}} Na^*\ (3p\ ^2P) + I^*\ (^2P_{1/2}), \qquad (2a)$$

or

$$NaI\ (X\ ^1\Sigma^+) \xrightarrow{?\ -\ 2100\text{Å}} Na^*\ (4s\ ^2S) + I\ (^2P_{3/2}). \qquad (2b)$$

Process (2a) would require a threshold energy shift relative to that of Eq. (1) of 7600 cm^{-1}; process (2b) would entail a corresponding shift of 8800 cm^{-1}. Indeed, this illustrates that the major obstacle to the extension of this NaI photodissociation technique to the study of quenching of more highly excited Na^* species arises because the density of NaI excited states correlating to different product atomic states increases rapidly with increasing excitation energy.

If the NaI vapor in vibrational level v and the zeroth rotational level is photodissociated by ultraviolet of frequency ν_o, then the kinetic energy E_v and speed u_v of recoil of Na^* relative to the center-of-mass (CM) of NaI are given by conservation of energy and linear momentum in terms of m_{Na}, m_I, and m_{NaI}, the masses of Na, I, and NaI, by

$$\frac{m_{Na}\, u_v^2}{2} = E_v = (m_I/m_{NaI})\, \varepsilon, \qquad (3)$$

$$\varepsilon = h\nu_o + \hbar\omega(v + \tfrac{1}{2}) - D_e - E^*.$$

In this equation, ω refers to the circular vibrational frequency of ground state NaI, D_e to its dissociation energy[24] (25310 cm^{-1}), and E^* to the Na^* ($3p^2P$) excitation energy (17000 cm^{-1}). Since, however, there exist thermal distributions in the NaI vibrational and rotational energies at a temperature T, the thermally averaged CM recoil energy and speed of Na^* may be taken as

$$\frac{m_{Na}\, u_T^2}{2} = E_T = E_{v=0} + (m_I/m_{NaI})(2kT). \qquad (4)$$

Finally, the final laboratory (LAB) Na^* velocity is obtained from the vector sum of the Na^* CM recoil velocity and the velocity of the original NaI molecule. Upon averaging the vector sums of the CM Na^* recoil velocity given in Eq. (4) and the randomly orientated most probable NaI thermal speed, $\bar{v}_{NaI} = (2kT/m_{NaI})^{1/2}$, the characteristic Na^* LAB speed is obtained[11] as:

$$V_T = u_T + \bar{v}_{NaI}^{\,2}/3\, u_T, u_T > \bar{v}_{NaI}\ ;$$

$$V_T = \bar{v}_{NaI} + u_T^2/3\, \bar{v}_{NaI}\ ,\ u_T < \bar{v}_{NaI}\ . \qquad (5)$$

In previous measurements of quenching cross sections by this photodissociative technique, the data has usually been analyzed[9] in terms of this characteristic LAB Na^* speed. In order to

proceed further and take into account the distribution of Na^* LAB speeds, it is necessary to first compound the thermal distributions in translational and rotational motions of the NaI in order to calculate the probability density function for LAB Na^* speeds, $P_{v,T,\nu_o}(V)$, produced by photodissociation of NaI in a particular vibrational level v by ultraviolet of frequency ν_o and infinitessimal bandwidth δ_ν. The full probability density function of Na^* speeds may then be calculated by summing the contributions of each vibrational level as

$$P_{T,\nu_o}(V) = \sum_{v=0}^{\infty} \rho_T(v)\ F_{T,\nu_o}(v)\ P_{v,T,\nu_o}(V). \qquad (6)$$

The first term, $\rho_T(v)$, is simply the thermal probability distribution function for NaI vibrational levels, readily calculated and shown in Fig. 4 for T = 633°C. The second factor is the relative probability of dissociation of an NaI molecule in vibrational level v by an ultraviolet photon of frequency ν_o, normalized such that

$$\sum_{v=0}^{\infty} \rho_T(v)\ F_{T,\nu_o}(v) = 1. \qquad (7)$$

In order to assess these $F_{T,\nu_o}(v)$ factors, it was necessary to reproduce the experimental reduced fluorescence curve shown in Fig. 3 by theoretical calculations. This was approached by recognizing that the steady-state rate of fluorescence of D-lines photons (I_D) was simply equal to the rate of excitation of NaI molecules, since Brus[11] has observed that NaI does not itself quench the Na^* fluorescence. In terms of an unknown apparatus

constant γ (comprised of photon detector efficiencies, efficiency of light collection, etc.), this is given by[25]

$$I_D = \gamma \frac{8\pi^3}{3h^2} |\mu|^2_{v,\nu_o} [NaI] I_{\nu_o}/c \tag{8}$$

where [NaI] is the number density of NaI vapor, I_{ν_o} is the ultraviolet flux per frequency interval so that I_{ν_o}/c is the corresponding ultraviolet energy density, and $|\mu|^2_{v,\nu_o}$ is the electronic dipole matrix element between the ground state of NaI in vibrational level v and an upper electronic state dissociating into Na^* and I with an unbounded nuclear wavefunction corresponding to an asymptotic radial kinetic energy of ε given by Eq. (3). The actual experimental quantity of interest is the reduced fluorescence $R_v(\nu_o) = I_D/P_{\nu_o}$ where P_{ν_o} is the absolute number of incident ultraviolet photons/sec, given in terms of the cross sectional area A_{ν_o} of the ultraviolet flux by $P_{\nu_o} = I_{\nu_o} \delta_\nu A_{\nu_o}/h\nu_o$. If the Franck-Condon principle is assumed[26] so that $|\mu|^2_{v,\nu_o}$ becomes a product of a constant electronic matrix element μ_e times an overlap integral $f_{v,\varepsilon}$ between the nuclear wavefunctions in the ground and excited states satisying the radial Schrödinger equation, the reduced fluorescence efficiency becomes

$$R_v(\nu_o) = \left[\frac{8\pi^3}{3hc} \frac{\gamma [NaI] |\mu_e|^2}{\delta_\nu A_{\nu_o}}\right] \frac{\nu_o f^2_{v,\varepsilon}}{\varepsilon^{1/2}} , \tag{9}$$

where the continuum nuclear wavefunctions are normalized asymptotically to sine functions of unit amplitude. Recognizing that the term in brackets in Eq. (9) is not a function of ν_o,

$R_v(\nu_o)$ is given to within a constant factor by $\nu_o f^2_{v,\varepsilon}/\varepsilon^{1/2}$. Furthermore, the $F_{T,\nu_o}(v)$ factors of Eq. (6) are proportional to this same variable, with a proportionality constant evaluated by means of Eq. (7). Finally, the theoretical calculations may be directly compared with experiment by summing over thermally distributed vibrational levels and integrating over the known bandpass function $M(\lambda,\lambda_o)$ of the monochromator as

$$R_T(\lambda_o) = c \sum_{v=0}^{\infty} \rho_T(v) \int_0^{\infty} M(\lambda,\lambda_o)\, R_v(c/\lambda)(d\lambda/\lambda^2). \qquad (10)$$

In order to calculate the reduced fluorescence curve shown in Fig. 3 by means of Eq. (10), the $X\ ^1\Sigma^+$ ground state of NaI was assumed to be described in the important region of r near its minimum by an ionic potential model,

$$V(r) = \beta \left[Ae^{-r/\rho} - \frac{e^2}{r} - \frac{e^2(\alpha_+ + \alpha_-)}{2r^4} - \frac{C_6}{r^6} - \frac{2e^2\,\alpha_+\alpha_-}{r^7} \right]. \qquad (11)$$

The polarizabilities of Na^+ and I^- were taken[27] as $\alpha_+ = 0.15$ Å^3 and $\alpha_- = 7.0$ Å^3 respectively and the dispersion force constant, C_6, was calculated from the Slater-Kirkwood approximation.[28] The repulsion constants, A and ρ, were evaluated by demanding that $dV/dr = 0$ at $r = r_e$ and fitting $(d^2V/dr^2)_{r=r_e}$ with the experimental force constant (data taken from Ref. 24). Maltz[29] has shown that this procedure provides a potential function which correctly accounts for the dipole moments and dipole derivatives of a number of alkali halides. Finally, the scaling factor β

was adjusted to 1.022 in order to obtain the correct dissociation energy for separation into Na^+ and I^-. Figure 4 shows a plot of the ground state potential function for NaI which was arrived at by fitting the expression given by Eq. (11) in the vicinity of the minimum where all of the vibrational levels of interest here were determined to a function which dissociated asymptotically into neutral Na + I.

The potential curve for the upper electronic state of NaI producing fluorescence for ultraviolet wavelengths from $\sim$ 2000 Å to $\sim$ 2500 Å was constrained to asymptotically approach a level 42300 cm^{-1} above the minimum of the ground state potential curve. Subject to this constraint, upper state potential curves were chosen by trial and error. The normalized bound ground state vibrational wavefunctions and continuous upper state functions (normalized to unit asymptotic amplitude) were evaluated by numerical integration of the radial Schrödinger equations and the corresponding Franck-Condon overlap integrals were evaluated numerically. Following this, reduced fluorescence curves were computed according to Eq. (10) and normalized to the experimental data shown in Fig. 3. Figure 3 shows the comparison at one temperature for the best agreement which was obtained, corresponding to the upper state potential curve shown in Fig. 4; similarly good fits were obtained for the data at other temperatures shown in Fig. 3. For purposes of illustration, it was assumed that the shorter ultraviolet wavelength fluorescence region shown in Fig. 3 was due to the process described in Eq. (2a). Assuming

that $|\mu_e|$ was the same for transitions to both upper states and that the potential curve for the state dissociating according to Eq. (2a) could be obtained simply by displacing the potential curve dissociating into $Na^* + I$ by the I^* excitation energy, the full theoretical reduced fluorescence curve shown in Fig. 3 was obtained. The agreement between this full theoretical curve and the experimental data is very good, although similar good agreement might also be obtained by fitting the higher energy data to a potential curve appropriate to Eq. (2b).

Previous calculations of Franck-Condon factors for transition from a bound state to an unbounded state have often resorted to approximating the continuous nuclear wavefunction of the upper state by a delta function centered at the classical turning point of the motion.[25] Auxiliary calculations on the potential curves shown in Fig. 4 with this delta function approximation for the upper state wavefunctions appreciably distort the calculated reduced fluorescence curves, resulting in much poorer agreement with experimental data than is obtained using the true continuum wavefunctions. Two previous studies[9,22] have also offered somewhat more qualitative forms for the first of the upper state potential curves shown in Fig. 4. While qualitatively of the same form as that shown in Fig. 4, backcalculations based on these potential curves showed much poorer agreement with the experimental data of Fig. 3.

In the following section, the Franck-Condon factors computed in fitting the data of Fig. 3 are used to estimate probability

density functions for speeds of photodissociatively produced Na^*. Before closing this section, however, it should be noted that the procedure adopted here of fitting the observed reduced fluorescence above $\sim$ 2100 Å by a single upper state potential curve is an approximation. Indeed, a number of considerations[12,23,30] indicate that this D-lines fluorescence is actually a consequence of absorptions to a number (or at least two) of rather closely spaced upper potential curves, all of which correlate asymptotically with $Na^*(3p\,^2P)$ and $I(^2P_{3/2})$. However, the Na^* speed distributions computed in the next section are not unduly sensitive to the forms of the Franck-Condon factors, so that the procedure adopted here should provide an excellent first approximation.

The Photodissociatively Generated Na^* Speed Distributions

The authors know of no general expression available in the literature for the distribution in speeds of the atomic products of the photodissociation of a diatomic molecule. Zare and Herschbach[30] did treat the more complex problem of the distribution in vector velocity of the Na^* produced by photodissociation of NaI; however, their distribution functions were arrived at by numerical computations and were based on the potential energy function given in Ref. 9. In this section, an analytic expression is derived for the probability density function, $P_{v,T,\nu_o}(V)$ of Eq. (6), of LAB Na^* speeds produced by photodissociation of an NaI molecule in vibrational level v with thermal distributions in translational and rotational energies. This is then combined

with the Franck-Condon factors discussed in the preceeding section to arrive at the full probability density function, $P_{T,\nu_o}(V)$ of Eq. (6). This is approached by assuming that the Na^* recoils away from the NaI center-of-mass at some one direction with a distribution of CM speeds u which is computed from the excess photon energy plus the NaI rotational energy which appears as radial recoil energy asymptotically. The distribution in LAB Na^* speeds for recoil events at this one CM angle is then obtained by considering the distribution in scalar values of $\vec{V} = \vec{u} + \vec{v}_{NaI}$ obtained by averaging over all of the values of the randomly oriented, thermally distributed, $\vec{v}_{NaI}$. This distribution in V is then subsequently employed to calculate the distribution in relative speeds of approach of Na^* to a foreign quenching gas M, i.e., the distribution in scalar lengths of

$$\vec{g} = \vec{V} - \vec{v}_M, \tag{12}$$

by averaging over the randomly orientated, thermally distributed values of $\vec{v}_M$. Thus, this procedure circumvents the far more complex problem treated in Ref. 30 of the distribution in angles of recoil of the Na^* relative to the incident direction of the ultraviolet flux.

The Distribution Function Ignoring Rotation

In order to assess the relative contributions of NaI translational and rotational energies to the breadth of the Na^* speed distributions, the $P_{v,T,\nu_o}(V)$ probability density function

is first computed for photodissociation of NaI molecules with no rotational angular momentum. Assuming then that the Na^* is produced with a recoil speed u_v given by Eq. (3) and directed along the z-axis, the center-of-mass Na^* recoil velocity distribution function for this case becomes

$$P_v^{J=0}(\vec{u}) = \delta(u_x)\ \delta(u_y)\ \delta(u_z - u_v). \tag{13}$$

Since the thermal distribution in NaI velocities is given in terms of the most probable thermal NaI speed, the corresponding distribution in LAB Na^* speeds becomes

$$P_{v,T,\nu_o}(\vec{V}) = \frac{\pi^{-\frac{3}{2}}}{\bar{v}_{NaI}^3} \int_{\vec{u}} P_v(\vec{u})\ e^{-v_{NaI}^2/\bar{v}_{NaI}^2} \left|\frac{\partial \vec{v}_{NaI}}{\partial \vec{V}}\right| d\vec{u}\ . \tag{14}$$

Recognizing that the Jacobian factor is unity for a Cartesian coordinate system, Eq. (14) is readily evaluated for the $P_v(\vec{u})$ function given in Eq. (13) to obtain:

$$P_{v,T,\nu_o}^{J=0}(\vec{V}) = \frac{\pi^{-3/2}}{\bar{v}_{NaI}^3}\ e^{-V^2/\bar{v}_{NaI}^2}\ e^{-u_v^2/\bar{v}_{NaI}^2}\ e^{\frac{2\,u_v V\cos\theta}{\bar{v}_{NaI}^2}} \tag{15}$$

in terms of θ, the polar angle between $\vec{u}_v$ and $\vec{V}$.

Equation (15) illustrates that the Na^* velocity distribution obtained in this case is simply the original NaI thermal velocity distribution with its origin now centered about $\vec{u}_v$. The corresponding speed distribution may now be obtained by transforming to spherical coordinates and integrating over solid angle, i.e.,

$$P_{v,T,\nu_o}(V) = \int_{\Omega} P_{v,T,\nu_o}(\vec{V})\ V^2 \sin\theta\ d\theta\ d\phi. \qquad (16)$$

This integral is readily evaluated to give a speed distribution function which is naturally expressed in terms of a reduced Na^* LAB speed $A = V/\bar{v}_{NaI}$ and reduced Na^* center-of-mass recoil speed $A_v = u_v/\bar{v}_{NaI}$ as

$$P^{J=0}_{v,T,\nu_o}(A) = \frac{2}{\pi^{1/2}} \frac{A}{A_v} e^{-A_v^2} e^{-A^2} \sinh 2AA_v. \qquad (17)$$

Figure 5 shows plots of this reduced speed probability density function for several Na^* CM recoil energies. The two highest recoil energies plotted (E_o = 10 kT and 30 kT) were not achieved in this experiment, but are plotted to illustrate the rather severe broadening introduced by the NaI thermal velocity spread even in the case of recoil energies much greater than thermal energies.

The expression given in Eq. (17) has actually been discussed in the literature previously. Thus, Chantry and Schulz[31] gave its high recoil energy limiting form in discussing the kinetic energy of negative ions formed in dissociative electron attachment to diatomic molecules. Stanton and Monahan[32] have also derived an expression identical to Eq. (17) in considering the kinetic energy distribution of fragment ions in a mass spectrometer. This probability density function is also identical to that of the distribution in relative collision speeds for a monoenergetic beam impinging upon a thermal gas sample in a scattering cell, and

in this context has been given in Ref. 33. Nevertheless, the derivation of Eq. (17) was presented here as a preliminary to the derivation of the probability density function obtained when the NaI rotational energy is included.

The Distribution Function Including Rotation

If the NaI molecule being phctodissociated possesses rotational energy E_r, this energy will appear as an increment to the recoil energy so that the resulting Na^* recoil speed will be given by

$$u^2 = u_v^2 + 2E_r/\kappa \tag{18}$$

where $\kappa = m_{Na}\, m_{NaI}/m_I$. Because of the small rotation constant and high temperature of the NaI vapor, the rotational energy may be treated as continuous and the rotational line strengths taken as unity so that the thermal probability density function for rotational energy becomes

$$P(E_r) = (kT)^{-1}\, e^{-E_r/kT}. \tag{19}$$

This leads to a distribution in Na^* CM recoil velocities directed along the z-axis which is obtained from Eq. (19) as

$$P_v(\vec{u}) = \frac{\kappa u_z}{kT}\, e^{\kappa u_v^2/2kT}\, e^{-\kappa u_z^2/2kT}\, \delta(u_x)\, \delta(u_y);\ u_z \geq u_v. \tag{20}$$

Inserting this expression into Eq. (14), the probability density function for Na^* LAB velocities becomes

$$P_{v,T,v_o}(\vec{V}) = \frac{\kappa}{kT}\, \frac{\pi^{-3/2}}{v_{NaI}^{-3}} \int_{-\infty}^{\infty}\int_{-\infty}^{\infty}\int_{u_v}^{\infty} u_z\, e^{\kappa u_v^2/2kT}\, e^{-m_{NaI} v_{NaI}^2/2kT} \times e^{-\kappa u_z^2/2kT}\, \delta(u_x)\, \delta(u_y)\, d\vec{u}. \tag{21}$$

Without attempting to evaluate this integral, the desired probability density function for Na^* speeds may be obtained by inserting it into Eq. (16). The resulting distribution function is naturally expressed in terms of reduced Na^* LAB speed B and reduced Na^* CM recoil speed B_v defined as

$$B = (1 + \eta)^{-1/2} V/\bar{v}_{NaI}, \tag{22}$$

$$B_v = (1 + \eta)^{1/2} u_v/\bar{v}_{NaI}$$

in terms of the mass ratio $\eta = m_{Na}/m_I$. The results are given in terms of the error function[34] as

$$P_{v,T,\nu_o}(B) = \eta(1 + \eta)^{1/2} B\, e^{(\eta/(1+\eta))B_v^2} e^{-\eta B^2} G(B,B_v)$$

$$\text{where } G(B,B_v) = \text{erf}(B+B_v) + \text{erf}(B - B_v),\ B > B_v, \tag{23}$$

$$G(B,B_v) = \text{erf}(B_v+B) - \text{erf}(B_v - B),\ B < B_v.$$

Figure 5 contrasts this speed distribution function obtained by including rotation with the simpler distribution obtained by ignoring effects of rotational energy and shows that the effects of rotational energy on the ensuing speed distribution may be appreciable for photodissociation near threshold. At very high recoil energies, however, Fig. 5 illustrates that the thermal diatomic translational energy is much more important than its rotational energy in determining the breadth of the speed distribution of the atomic product. This effect arises because the

rotational energy always adds to the recoil speed impacted by absorption of a photon whereas the translational velocity of the center-of-mass may add to or subtract from the CM recoil velocity.

The full probability density functions for Na^* speeds produced photodissociatively in this work were calculated by means of Eqs. (23) and (6) and the Franck-Condon factors computed in the preceeding section. The results of convoluting these distribution functions with the bandpass function of the monochromator are shown in Fig. 6. The curves of Fig. 6 are not unduly broadened relative to those of Fig. 5,indicating that the thermal distribution of NaI vibration energy was not a major source of breadth of the Na^* speed distribution. Moreover, the curves of Fig. 6 illustrate that the 47 Å FWHM monochromator bandpass employed in the quenching studies had only a minor effect on the energy resolution obtained. In calculating averaged collisional quenching cross sections for comparison with experimental data, the probability distribution functions of interest are those for the relative collision speed g of Eq. (12). These distribution functions were calculated numerically by compounding the calculated, monochromator-bandpass-averaged Na^* speed distributions with the thermal distribution in velocities of the quenching gases. Examples of these computed relative collision speed distribution functions for collision of Na^* with a gas of much greater mass (I_2) and of comparable mass (C_2H_4) are shown in Fig. 6 and illustrate that this is another very important source of loss of

energy resolution in the quenching studies in the case that the quenching gas has a mass comparable to or less than that of the species being quenched.

The Steady-State Na^* Speed Distributions

The Na^* speed distributions produced by photodissociation of NaI which were computed in the preceeding section are certainly not precisely the true steady-state Na^* speed distributions because of possible relaxation of the original distributions as a consequence of collisions between the Na^* and other gas molecules which do not destroy the Na^* electronic excitation but may alter its speed. These collisions may be either elastic or inelastic, but certainly the elastic collisions will be of dominant importance in relaxing the Na^* speed owing to their higher probability of occurence. The derivation of the true steady-state distribution is a difficult problem, beyond the scope of the present study. Nevertheless, this section offers some estimates of the likely magnitudes of the differences between the steady-state Na^* LAB speed distributions and the photodissociatively generated distributions.

The cross section Q_R and associated rate constant $k_R = g\ Q_R$ for this relaxation by elastic collisions is dependent on the extent of perturbation of the Na^* speed, V, considered. Thus, small impact parameter hard collisions may appreciably alter V, but these occur with a correspondingly small rate constant. On the other hand, large impact parameter collisions will occur much

more frequently, but will produce a correspondingly smaller perturbation of V. Suppose then that the relaxation is characterized by some cross section $Q_R = \pi b_R^2$. If this is big, it will include contributions of some small impact parameter hard collisions, but will be dominated by larger impact parameter collisions for which $b \lesssim b_R$. Now, let k^* represent the rate constant for the first order decay of electronic excitation of Na^*. Then, k^* will be given in terms of the rate constants for spontaneous emission of Na^*, k_r, and for collisional quenching of Na^*, k_q, by

$$k^* = k_r + k_q[M] \tag{24}$$

where [M] is the quenching gas number density. Thus, the probability that an Na^* atom will experience it at least one elastic collision during its lifetime is given by $k_R[M]/(k^* + k_R[M])$.

In analyzing the problem further, it is natural to divide it into two regimes, that of high and low pressures of quenching gas, because the true steady-state Na^* speed distribution will be dependent on pressure. In the low pressure regime, k^* is essentially given by k_r, known[11] to have the value of 6.2×10^7 sec^{-1}. Taking 1 Torr of quenching gas as typical of this regime, this implies that k_R must be $\sim 6 \times 10^{-9}$ cm^3 sec^{-1} in order that 50% of the Na^* atoms experience at least one elastic collision during their lifetime. This corresponds to impact parameters b_R for the elastic collisions of $\sim$ 14, 12, and 10 Å for relative collision speeds of 1.0, 1.5, and 2.0 km/sec. At these large

impact parameters, the collision is dominated by the long range form of the potential. Taking this long range form to vary as C_6/r^6, the high energy approximation for the classical elastic angle of deflection which should adequately describe these soft collisions gives

$$\chi \approx 15\pi\ C_6/8\mu g^2 b^6 \tag{25}$$

in terms of the reduced mass of the collision partners, $\mu = m_{Na}m_M/(m_{Na}+m_M)$. If C_6 is assumed to be $\sim -10^{-57}$ erg-cm^6, this predicts very small angles of deflection, $\sim -0.2 - -.3°$ for these collisions.

The velocity of the quenching gas is distributed thermally; however, the effect of the average collision may be estimated by assuming that the two gases intersect as right angles and assigning to the foreign gas its most probable thermal speed, $\bar{v}_M$. In this case, the following small angle approximation may be used to estimate the perturbation (ΔV) of the Na^* speed:

$$\Delta V/V = \pm\ \chi(m_M/(m_M+m_{Na}))(\bar{v}_M/V). \tag{26}$$

For these small deflection angles, Eq. (25) provides estimates of 0.1 - 0.2% perturbations in V. Thus, at low pressures of quenching gas ($\sim$ 1 Torr), the average elastic collision perturbs the Na^* speed negligibly. Of course, virtually all of the Na^* atoms may experience several elastic collisions which are even softer than those considered in the preceeding paragraph. However, the effect of each of these very soft collisions will be very

small. Moreover, they are about equally likely to increase or decrease V, so that the net spread in V might be expected to vary something as the square root of the number of these very soft collisions.

While these considerations suggest that the nascent Na^* speed distributions are negligibly perturbed for low quenching gas pressures, the actual data on quenching cross sections was collected for quenching gas pressures in the range of $\sim$0.5 - 10 Torr. In the high pressure limit, k^* is dominated by $k_q[M]$ so that the condition that half of the Na^* atoms experience a relaxation collision prior to quenching becomes $Q_R = Q_q$. Recognizing, however, that the quenching collisions are probably given by the smaller impact parameter collisions, we may estimate that $Q_q = \pi b_q^2$. Then the important relaxation collisions will occur for impact parameters larger than this so that

$$Q_R = \pi(b_R^2 - b_q^2).$$

Thus, the 50% relaxation collision is characterized by an impact parameter $b_R = \sqrt{2}\, b_q$. Taking benzene as an example and anticipating the results of the following section on the magnitude of the quenching cross section, Eqs. (25) and (26) suggest a deflection angle of $\sim$ 3° and fractional perturbation of V of $\sim$ 1 - 2%. Of course, these are no longer extremely soft collisions and Eq. (25) is not strictly applicable, but should provide an adequate approximation.

Here again, this calculated small perturbation of V is encouraging, but may be somewhat misleading in this case. Thus, the probability that the Na^* will suffer a hard collision is somewhat higher in this high pressure limit. For example, it seems probable that $\sim$ 10% of the Na^* atoms may suffer a collision which could change V by as much as 50%. Nevertheless, it would appear that even at this high pressure limit, the true Na^* speed distribution will resemble that calculated for photodissociation of NaI, but with some additional breadth and a slight downward shift of the most probable Na^* speed. In what follows, the quenching cross sections are analyzed in terms of the unrelaxed Na^* speed distributions and this procedure is further supported by the observation that the high energy data evaluated in this study agree well with other results in the literature when extrapolated down to thermal energies.

DATA ANALYSIS AND RESULTS

If it is assumed that absorption of an incident photon by NaI vapor leads directly to production of an Na^* as described by Eq. (1) and if it is further assumed that the Na^* formed must either radiate or be collisionally quenched by the foreign gas present in the cell, the Stern-Volmer relation is obtained[9] for the ratio of the reduced fluorescence efficiency for finite quenching gas, $R_{[M]}$, to that for no quenching gas, R_0:

$$\frac{R_0}{R_{[M]}} = 1 + (k_q/k_r)[M]. \qquad (27)$$

Figure 7 shows this ratio as a function of ethylene gas pressure for four typical ultraviolet wavelengths studied. Also shown are least squares fits of the data for each wavelength to Eq. (27). It will be noted that the zero pressure intercepts of these least squares linear fits differ slightly from the value of unity predicted by Eq. (27). In all cases, however, this discrepancy in the intercept is less than the standard derivation in the intercept provided by the least squares fit. The rest of the primary data collected for ethylene as well as that collected for the other six quenching gases studied is not presented here. However, the data shown in Fig. 7 is typical of the quality of the data obtained for all of the quenching gases, with the possible exceptions of I_2 where the inherent room temperature vapor pressure of this material limited measurements to low quenching gas pressures and consequent D-lines fluorescence ratios near unity.

If it is assumed for purposes of an initial analysis of the data that the quenching cross section is energy independent over the spread in relative collision velocities and that the Na^* is produced with the one characteristic speed V_T given by Eq. (5), then the quenching rate constant may be shown to be given in terms of $x = V_T/\bar{v}_M$ as

$$k_q = \pi^{-1/2} \langle Q_q \rangle \bar{v}_M \, \psi(x)/x$$

$$\text{where } \psi(x) = x\, e^{-x^2} + (2x^2 + 1) \int_0^x e^{-y^2} dy. \qquad (28)$$

Quenching cross sections for the Na^* + C_2H_4 collision evaluated from measured values of k_q by means of Eq. (28) are plotted in Fig. 7 against the characteristic relative speed, $\wedge$

$$<g> = V_T + \bar{v}_M^2/3V_T, \quad V_T > \bar{v}_M$$
$$<g> = \bar{v}_M + V_T^2/3\bar{v}_M, \quad V_T < \bar{v}_M. \tag{29}$$

The error bars shown reflect only the standard deviations in k_q provided by the least squares fits of the data to Eq. (27). Other sources of error certainly exist. For example, if the NaI dissociation energy employed here were in error, this could significantly alter the calculated values of $<Q_q>$ and $<g>$, although this would have less effect on the functional dependence of $<Q_q>$ on $<g>$ shown by the data.

Figures 8 and 9 give similar plots of phenomenological values of $<Q_q>$ versus characteristic relative collision speed. Because SO_2 and C_6H_6 absorbed the shorter wavelength ultraviolet somewhat, a correction has been applied in arriving at the higher velocity data points plotted in Fig. 8 for these two gases. The magnitude of the correction was relatively uncertain, resulting in larger uncertainties in the data points plotted at higher velocities than are indicated by the error bars shown. This additional uncertainty was smaller than the standard deviations of the least squares fits to Eq. (27) in the case of benzene, but comparable for the SO_2 data at higher collision speeds.

The Stern-Volmer steady-state procedure for measurements of the quenching cross sections which is employed here is open to criticism because of its assumption of a very limited chemistry in the hot NaI-quenching species vapor mixture. The pulsed ultraviolet excitation followed by observation of the rate of decay of the subsequent Na^* fluorescence which was employed in Ref. 11 to measure the I_2 quenching cross sections is a more direct method and is not subject to the possible criticisms of the Stern-Volmer technique. Unfortunately, this experimental method is much more time consuming and so was not adopted in this study. Figure 9 shows the very excellent agreement between the $Na^* + I_2$ quenching cross sections measured in this study (if the data analysis method employed in Ref. 11 is used) and the values arrived at in Ref. 11 by the more direct pulse technique. The relatively large error bars shown on our data points in Fig. 9 are a consequence of the limited I_2 vapor pressure region scanned. The $Na^* + CO_2$ quenching cross section data shown in Fig. 8 is also in similar good agreement with the values measured in Ref. 9 by the same Stern-Volmer technique employed here, if our data is analyzed by the procedure employed in Ref. 9.

In attempting to deconvolute the experimental data to arrive at the true dependence of the quenching cross sections on relative energy, it was assumed that the cross sections varied as $K_s/g^{(4/s)}$ with s = 4, 5, or 6. As discussed in the following section, there are varying theoretical grounds for expecting that Q_q might vary in this manner. However, the main reasons for fitting the data

to these functions were (1) that adequate fits to the experimental data were obtained and (2) that comparisons of the fits obtained with s = 4, 5, and 6 provided some estimate of the sensitivity of the experimental data to the precise form of $Q_q(g)$. Having assumed a form of $Q_q(g)$, the quenching rate constant was calculated by numerical integration over the monochromator-bandpass-averaged probability density function for relative collision speeds derived in a previous section as

$$k_q = \int_0^\infty g\, Q_q(g)\, P_{T,\nu_o}(g)\, dg. \tag{30}$$

Phenomenological values of $\langle Q_q \rangle$ were then calculated from these computed values of k_q from Eq. (28) for comparison with the data points. Figure 7 shows the $K_5/g^{(4/5)}$ and $K_6/g^{(2/3)}$ forms of $Q_q(g)$ together with their energy averaged phenomenological quenching cross sections which best fit the ethylene data. Table I gives the K_4, K_5, and K_6 constants which best fit the experimental data for all seven quenching gases studied and Figs. 8 and 9 show the corresponding fits to the data obtained for the other six gases. In general, adequate fits are obtained for s = 4, 5, or 6. The data seem to show some predilection for s = 6 except for the CH_3CN quenching gas, where s = 4 appears to provide the best fit.

DISCUSSION

Comparison with Other Work

The good agreement between the quenching cross sections obtained in this work and those derived by similar NaI photo-

dissociative studies for I_2 (Ref. 11) and CO_2 (Ref. 9) has already been noted in the previous section. Most of the results of earlier workers employing the NaI photodissociative technique are discussed in Refs. 9 and 11 and so are not considered here. However, one other more recent study[10] by this technique provided cross sections for quenching of Na^* by CO_2 and CH_3CN which are about a factor of two higher than those reported here. We cannot account for this discrepancy, but note again our agreement with Hanson's[9] results for CO_2.

In addition to comparisons of the present work with previous studies employing the NaI photodissociation technique, it is also of interest to compare these results with thermally averaged rate constants for quenching of Na^* obtained by mixing Na vapor with quenching gases. The results of all such previous thermal studies for the quenching gases examined here are listed in Table II. Indeed, one previous criticism[35] of the NaI photodissociative technique has been the inability to unequivocally compare the results obtained on quenching cross sections with thermal quenching rate constants. However, it has been argued in this work that the distribution in relative collision speeds is known and this has been used to fit the data to functional dependences of the form $Q_q(g) = K_s/g^{(4/s)}$. If this functional form is assumed to hold down to the lower collision speeds encountered in some of the thermal experiments, then thermal rate constants may be calculated from the expressions given in Ref. 39.

Table II compares literature values of thermal quenching rate constants with the extrapolations of the $K_6/g^{(2/3)}$ form of $Q_q(g)$ employed here. The first entry in the table for benzene (Ref. 36) was obtained by a pulsed excitation study of the lifetime of Na^* fluorescence and so should be especially reliable. The C_6H_6 and C_2H_4 results reported in Ref. 37 were obtained by a steady-state resonance fluorescence technique and so are subject to possible ambiguities occasioned by imprisonment of resonance radiation and collisional broadening of the resonance absorption line. Indeed, comparisons of the results of Refs. 36 and 37 for N_2, H_2, CO_2, and C_6H_6 suggest that the results of Ref. 37 may be too high by about a factor of two. In view of this, the agreement shown in Table II between the results of the present work and thermal literature values for C_6H_6 and C_2H_4 is gratifying. Extrapolations of the K_4/g or $K_5/g^{4/5}$ fits obtained here would give higher values of $10^{10}k_q$ ($\sim$ 11 and 13 for s = 5 and 4) for C_6H_6 in poorer agreement with the literature values, although the change in going from s = 6 to s = 5 is not too pronounced. These comparisons and the data presented earlier suggest that $Q_q(g)$ varies as $g^{-(0.8 \pm 0.6)}$ for a speed range of $\sim$ 0.7 - 2.0 km/sec for benzene and ethylene as quenching gases. The agreement between the CO_2 result obtained here and that obtained from studies of fluorescence in a flame reported in Ref. 35 is very good. Since the flame temperature was high, the characteristic thermal collision speed shown in Table II is comparable to those directly studied here, so that calculations of k_q for the s = 4, 5, or 6

fits would all yield comparable values. The magnitude of k_q arrived at in Ref. 38 by a flame fluorescence study is in rather bad agreement with that obtained here; these workers also seemed to observe a g^{-2} dependence of Q_q for $Na^* + CO_2$, in clear disagreement with the results shown in Fig. 8.

Theoretical Implications

The Weak Quenchers

The data obtained here for CO_2, C_2H_4, CH_3CN, CF_3Cl, and C_6H_6 are well fit by quenching cross sections of the form $Q_q(g) = K_s/g^{(4/s)}$ with s = 4 - 6. This is the well known functional form of the cross section which is obtained by assuming that a constant fraction w of those incoming trajectories which surmount the barrier in the effective potential, obtained by adding the centrifugal repulsion to the true long-range potential $V(r) = C_s/r^s$, lead to quenching collisions. This model provides[39] an expression for $Q_q(g)$ in terms of the power law potential constant,

$$Q_q(g) = w\pi\left[\frac{s}{s-2}\right]^{\frac{s-2}{s}}\left[\frac{s}{\mu}\right]^{2/s}\frac{C_s^{2/s}}{g^{4/s}} \quad . \tag{31}$$

The Na^* atoms involved in these collisions will experience electric quadrupole interactions. This could give rise to a long-ranged r^{-4} dipole-quadrupole potential for collisions with the polar quenching gases. However, this interaction would average to zero over one rotational period of the quenching molecule except in the case of symmetric top molecules with rotation about the

symmetry axis excited. Moreover, no qualitative difference in behavior between the polar and non-polar quenching gases was observed here, so that the dipole-quadrupole interaction does not appear to be dominant in general in determining the quenching cross sections. It may influence the CH_3CN collisions somewhat. This molecule does possess the largest dipole moment of the seven quenching gases studied here, and the energy dependence of its quenching cross section shown in Fig. 8 is somewhat steeper than is that of the other quenching gases. All of the quenching gases studied here should have electric quadrupole moments. Thus, this should give rise to long range r^{-5} quadrupole-quadrupole interactions. Although the N_2^* quadrupole moment is apparently not known, our estimates indicate that these quadrupole-quadrupole interactions should be less than or at most comparable to the r^{-6} dispersion interactions at internuclear separations important in determining the barriers in the effective potentials.

Various approximations have been employed to estimate the C_6 dispersion force constant. Analysis of these approximations in Ref. 28 indicates that the dispersion contribution to C_6 should be well described by the Slater-Kirkwood approximation for these collisions; the dipole-induced dipole contribution should be much smaller and will be ignored. For this case of an excited alkali atom with one electron in the outer shell of polarizability α_1 much greater than the polarizability α_2 of the quenching gas, the Slater-Kirkwood approximation for C_6 provides the following approximation for $Q_q(g)$ from Eq. (31) in terms of e and m_e, the

charge and mass of the electron:

$$Q_q(g) = w \frac{3\pi}{2} \left[\frac{6e\hbar}{m_e^{1/2}}\right]^{1/3} \frac{\alpha_1^{1/6} \alpha_2^{1/3}}{\mu^{1/3} g^{2/3}}. \quad (32)$$

Note that this expression predicts that for constant w, α_1, and g, the quenching cross section should vary as $(\alpha_2/\mu)^{1/3}$. This differs considerably from the older suggestion[40] that Q_q should scale as $\alpha_2\mu^{1/2}$ and the more recent suggestion[40] that the quenching of electronic excitation in molecules proceeds by a molecular predissociation so that Q_q should vary as $\mu^{1/2}\ I_2\ \alpha_2/R_x^3$, where I_2 is the ionization potential of the quenching species and R_x is mean distance of closest approach of the collision pair.

Table III provides a comparison of the K_6 coefficients measured here with estimates provided by Eq. (32) for w = 1 and α_1[41] = 51 Å^3, and indicates that Eq. (32) (with w=1) does provide reasonable estimates of the magnitude of the quenching cross sections for the weaker quenchers studied here.[42] The K_6 values estimated from Eq. (32) may be slightly in error because of approximations involved in arriving at values of C_6; however, these errors should be small because K_6 depends only on the cube root of C_6. Thus, the entries in Table III clearly imply w < 1 for CO_2, C_2H_4, and C_6H_6. Indeed, the results obtained here in conjunction with earlier work[5-11,35-38] suggest that most of the molecules which quench Na^* electronic excitation may be broadly divided into four classes. In class A may be listed those molecules which cannot chemically react with Na^* because all reaction

channels are either endoergic or essentially thermoneutral (for which an appreciable activation energy might be expected), and whose lowest unfilled molecular orbital is a very high energy, antibonding σ^* orbital. Examples of molecules in this class, such as CF_4, saturated alkanes, and possibly H_2O, are all very inefficient quenchers. In class B are included those molecules which cannot chemically react with Na^*, but which possess relatively low lying unfilled π^* molecular orbitals. These molecules, examples of which are provided by the CO_2, C_2H_4, and C_6H_6 studies here, are relatively efficient quenchers, with w values evaluated from Eq. (32) between 0.1 and 1.0. Since no change in chemical identity is effected by these quenching collisions, the Na^* excitation energy must be dissipated either as translational recoil energy or as internal excitation of the class B quenching molecule. Studies of the chemiluminescence[43] produced by the Na^* + CO quenching collision and of the inverse collisions using vibrationally[44,45] or translationally[46] hot species suggest that the electronic excitation is released predominately as internal (vibrational) excitation of the quenching molecule. Class C would include quenching molecules which, while not strongly electron-negative, afford a very exoergic reaction channel. Results for two molecules of this class studied here, CH_3CN and CF_3Cl, suggest that their quenching cross sections may be given by Eq. (32) with w = 1, although results for many more molecules of this class will be required to unequivocally establish this. Finally, Class D quenchers, examplified by the I_2 and SO_2 behaviors observed in

this work, are highly electronegative and exhibit quenching cross sections which are too large to be in interpreted in terms of the long range dispersion forces between the neutral reactants.

Thus, the quenching behavior observed in this study suggest that the long-range dispersion forces may account for the magnitude and energy dependence of quenching of Na^* $(3p\,^2P)$ by Class C and, to a certain extent, Class B quenchers. Nevertheless, many additional studies will be required to unequivocally establish the role of these dispersion forces. In particular, experiments are underway in our own laboratory to measure quenching cross sections of more highly excited ^2P states of alkali metal vapors. Thus, calculations reported in Ref. 41 indicate that the magnitude of the polarizability of a ^2P state of an alkali metal increases by about an order of magnitude for each increment of one in the principal quantum number of the outer p electron. Even more striking is the fact that for Na^*, the polarizability changes sign on going from the $3p\,^2P$ to the $4p\,^2P$ state, so that the dispersion forces should be repulsive for collisions of Na^* $(4p\,^2P)$ and Na^* $(5p\,^2P)$ with foreign gas molecules.

The Stronger Quenchers

Table III indicates that SO_2 and I_2 exhibit cross sections for quenching of Na^* $(3p\,^2P)$ which are too large to be understood in terms of the centrifugal barrier in the effective potentials associated with the long-range dispersion forces between the neutral reactants. Thus, these large quenching cross sections demand a strong force which pulls the reactants into small inter-

nuclear separation and which is operative at very long distances. This requisite long-range force has long been understood[17a] in terms of an electron transfer model. In this model, the incoming Na^* atom is seen to transfer its electron to the quenching gas at a distance R_c where the coulombic potential curve for the two ions becomes lower than that for the two neutrals, and the resulting coulombic force rapidly accelerates the ion pair formed to small internuclear separations. In terms of the ionization potential of Na^*, I_1, and the electron affinity of the quencher, EA, R_c is given to lowest order by $e^2/(I_1 - EA)$.

The electron affinity of SO_2 is reported to be[47] $\sim$ 1.1 ev. so that the crossing point, R_c, occurs at a relatively small internuclear separation, $\sim$ 7.5 Å, in the $Na^* + SO_2$ collision. Moreover, Table III indicates that the NaO + SO reaction channel is closed by energy conservation, at least at the lower relative collision speeds studied here. Thus, this quenching collision is pictureed as taking place by a Franck-Condon transitions from SO_2 to SO_2^- at R_c, exciting vibrational levels of SO_2^- on the incoming trajectory. The $Na^+ - SO_2^-$ ion pair formed then may oscillate many times, passing through crossing points with the $Na^* + SO_2$ and $Na + SO_2$ potential curves. In each passing, the SO_2^- may re-transfer the electron to Na^+, at the same time making Franck-Condon transitions to various vibrational levels of SO_2. Calculations on the quenching of Na^* by N_2 by this model are presented in Ref. 48 and suggest that it may provide an efficient mechanism for the dissipation of the Na^* electronic excitation in vibrational excitation of SO_2

and recoil energy of Na from SO_2.

A recent measurement[49] indicates a relatively large electron affinity for I_2, 2.6 e.v., corresponding to a calculated $Na^* + I_2$ ionic curve crossing radius of $\sim$ 36.5 Å. Table III indicates that this quenching collision can proceed by the very exoergic reaction forming NaI + I; indeed, the exoergicity is such that the reaction products might even be[11] Na + I + I. This suggest that any incoming $Na^* + I_2$ trajectories which successfully cross onto the ionic curve have a very high probability of exiting in the reactive channel. In view of this, the observation that the $Na^* + I_2$ quenching cross section measured here is very much less than πR_c^2 is understood in terms of a very low probability that the Na^* will transfer its electron over the large distance required while the Na - I_2 internuclear separation is in the vicinity of the curve crossing radius. This same Born-Oppenheimer breakdown effect has recently been discussed[50] in rationalizing the observed branching ratios for thermal dissociation of alkali halide vapors between atoms and ions. Moreover, Child[51] has derived an expression for the translational energy dependence of the cross section for reactions such as $Na^* + I_2$ by calculating the probability of a transition between the neutral and ionic curves as a function of the local radial velocity at R_c. Although his calculations did not extend to the very large crossing radius encountered here, extrapolation of his reported calculations is in qualitative agreement with the magnitude and velocity dependence of the $Na^* + I_2$ quenching cross section measured here.

ACKNOWLEDGEMENTS

We are indebted to Thomas Weber and Maynard Chen who collaborated on parts of the work described here during their senior undergraduate years in the College of Chemistry: Mr. Weber helped in the original assembly of the equipment, especially the development of the H_2 arc continuum source; Mr. Chen assisted in the measurements of many of the quenching cross sections presented here. This work was supported by the U.S. Atomic Energy Commission through the Lawrence Berkeley Laboratory.

REFERENCES

1. A. Terenin, Z. Physik. 37, 98 (1926).
2. For a review, see: G.G. Neuimin, "Photodissociation of Salt Molecules in the Gaseous State" in Elementary Photoprocesses in Molecules, B.S. Neporent, Ed. (Consultants Bureau, New York, 1968), p. 3.
3. V.A. Dudkin, V.I. Malyshev, and V.N. Sorokin, Opt. Spectrosc. 20, 313 (1966).
4. J.A. Bellisio and P. Davidovits, J. Chem. Phys. 53, 3474 (1970).
5. J.G. Winans, Z. Physik 60, 631 (1930).
6. A. Terenin and N. Prileshajewa, Z. Physik. Chem. (Leipzig) B13, 72 (1931).
7. B. Kisilbach, V. Kondratjew, and A. Leipansky, Physik. Z. Sowjetunion 2, 201 (1932).
8. V. Kondratjew and M. Siskin, Physik. Z. Sowjetunion 8, 644 (1935).
9. H.G. Hanson, J. Chem. Phys. 23, 1391 (1955).
10. D.J. Dowling, G.R.H. Jones, and E. Warhurst, Trans. Faraday Soc. 55, 537 (1959).
11. L.E. Brus, J. Chem. Phys. 52, 1716 (1970).
12. In a related experiment, H.G. Hanson, J. Chem. Phys. 27, 491 (1957) measured velocity dependent cross sections for interconversion of the Na^* $3p\,^2P$ fine structure components.
13. J. Gatzke, Z. Physik. Chem. (Leipzig) 223, 321 (1963).
14. N. Prileshajewa, Physik. Z. Sowjetunion 2, 351, 367 (1932).
15. N. Prileshajewa, Acta Physicochim. URSS 2, 647 (1935).
16. D.J. Dowling and E. Warhurst, Trans. Faraday Soc. 55, 532 (1959).

17. See, for example, the following reviews: (a) D.R. Herschbach, Advan. Chem. Phys. 10, 319 (1966); (b) E.F. Greene and J. Ross, Science 159, 587 (1968); (c) J.P. Toennies, Ber. Bunsenges. Physik. Chem. 72, 927 (1968).

18. J.A.R. Samson, Techniques of Vacuum Ultraviolet Spectroscopy (John Wiley and Sons, New York, 1967).

19. G. Herzberg, Molecular Spectra and Molecular Structure. III. Electronic Spectra and Electronic Structure of Polyatomic Molecules (Van Nostrand Reinhold Company, New York, 1966).

20. N.A. Finkelstein, Rev. Sci. Instr. 21, 509 (1950).

21. G. Herrmann and S. Wagner, The Oxide Coated Cathode (Chapman & Hall, London, 1951), pp. 20, 33, 58ff.

22. P. Davidovits and D.C. Brodhead, J. Chem. Phys. 46, 2968 (1967).

23. H.G. Hanson, J. Chem. Phys. 47, 4773 (1967).

24. L. Brewer and E. Brackett, Chem. Rev. 61, 425 (1961).

25. A.S. Coolidge, H.M. James, and R.D. Present, J. Chem. Phys. 4, 193 (1936).

26. Auxilliary $\overline{r}$-centroid calculations indicate that the assumption of the Franck-Condon principle introduces only very small errors here.

27. A. Dalgarno, Advan. Phys. 11, 281 (1962).

28. H.L. Kramer and D.R. Herschbach, J. Chem. Phys. 53, 2792 (1970).

29. C. Maltz, Chem. Phys. Letters 3, 707 (1969).

30. (a) R.N. Zare and D.R. Herschbach, Proc. IEEE 51, 173 (1963); (b) R.N. Zare and D.R. Herschbach, Lawrence Radiation Laboratory Report UCRL-10438, Berkeley, Cal., 1963.

31. P.J. Chantry and G.J. Schulz, Phys. Rev. Letters 12, 449 (1964).

32. H.E. Stanton and J.E. Monahan, J. Chem. Phys. 41, 3694 (1964).

33. Fr. von Busch, H.J. Strunck, and Ch. Schlier, Z. Physik. 199, 518 (1967).

34. Handbook of Mathematical Functions, National Bureau of Standards Applied Mathematics Series 55, M. Abramowitz and I.A. Stegun, ed. (U.S. Government Printing Office, Washington, D.C., 1964).

35. D.R. Jenkins, Proc. Roy. Soc. (London) A 293, 493 (1966).

36. C. Bästlein, G. Baumgartner, and B. Brosa, Z. Physik. 218, 319 (1969).

37. R.G.W. Norrish and W.M. Smith, Proc. Roy. Soc. (London) A 176, 295 (1940).

38. H.P. Hooymayers and C.T.J. Alkemade, J. Quant. Spectrosc. Radiat. Transfer 6, 847 (1966).

39. H.S. Johnston, Gas Phase Reaction Rate Theory (The Ronald Press Co., New York, 1966) pp. 142-145.

40. For a recent review of quenching, see: J.I. Steinfeld, Accts. Chem. Res. (1970), 313.

41. R.W. Schmieder, A. Lurio, and W. Happer, Phys. Rev. A 3, 1209 (1971).

42. The polarizabilities used are averaged over orientations and the minor effects due to the anisotropies of the polarizabilities of Na^* and the quenching gases are neglected.

43. J.C. Hassler and J.C. Polanyi, Disc. Faraday Soc. 44, 182 (1967).

44. J.E. Mentall, H.F. Krause, and W.L. Fite, Disc. Faraday Soc. 44, 157 (1967).

45. S. Tsuchiya and I. Suzuki, J. Chem. Phys. 51, 5725 (1969).

46. V. Kempter, W. Mecklenbrauck, M. Menzinger, G. Schuller, D.R. Herschbach, and Ch. Schlier, Chem. Phys. Letters 6, 97 (1970).

47. K. Kraus, W. Muller-Dzysing, and H. Neuert, Z. Naturforsch. 16a, 1385 (1961).

48. E. Bauer, E.R. Fischer, and F.R. Gilmore, J. Chem. Phys. 51, 4173 (1969).

49. J.J. De Corpo and J.L. Franklin, J. Chem. Phys. 54, 1885 (1971).

50. J.J. Ewing, R. Milstein, and R.S. Berry, J. Chem. Phys. 54, 1752 (1971).

51. M.S. Child, Mol. Phys. 16, 313 (1969).

Table I. Best Experimental Values[a] of K_s for Na^* Quenching Cross Sections Varying as $K_s/g^{4/s}$

Quenching Gas	$10^9 K_4$	$10^{10} K_5$	$10^{11} K_6$
CO_2	0.88	0.78	1.6
C_2H_4	0.93	0.82	1.7
CH_3CN	1.2	1.1	2.3
CF_3Cl	1.2	1.1	2.2
C_6H_6	1.3	1.2	2.4
SO_2	1.8	1.6	3.3
I_2	2.9	2.6	6.0

[a] K_s is given in units of cm^2-$(cm/sec)^{4/s}$.

Table II. [a]Comparison of Thermal Quenching Rate Constant Measurements with Extrapolations of $K_6/g^{2/3}$ Fit

Quenching Gas	Ref.	T(°K)	g_T	$10^{10}k_q$ Reported	$10^{10}k_q$ This work
C_6H_6	36	~600	0.85	8.0	10
C_6H_6	37	400	0.69	16	10
CO_2	35	1600	1.49	7.5	8.2
CO_2	38	1790	1.58	17	8.4
C_2H_4	37	400	0.82	11	7.1

[a] Rate constants are given in cm^3/molecule-sec. The average relative collision speeds, $g_T = (8kT/\pi\mu)^{1/2}$, are given in units of km/sec.

Table III. Comparisons of Measured Na^* Quenching Cross Sections with Projections Based on Long Range Dispersion Forces

	CO_2	C_2H_4	CF_3Cl	CH_3CN	C_6H_6	SO_2	I_2
Reaction Product	NaO	NaH	NaCl	NaCN	NaH	NaO	NaI
ΔD_o [a]	-10	∿-8	66	∿46	∿-8	-14	85
μ(gms/mole)	15.3	12.6	18.9	14.7	17.8	16.9	21.1
$\alpha_2(Å^3)$ [b]	2.6	4.3	5.0	4.4	10.3	3.7	9.7
$10^{11}K_6$(theo) (Eq. 32)	2.0	2.5	2.2	2.4	2.9	1.7	2.7
$10^{11}K_6$(exp.) (Table I)	1.6	1.7	2.2	2.3	2.4	3.3	6.0

[a] $\Delta D_o = D_o(Na-X) + E^* - D_o(R-X)$ is the reaction exoergicity. $D_o(Na-O)$ taken from and $D_o(Na - CN)$ estimated from arguments given in R.R. Herm and D.R. Herschbach. J. Chem. Phys. 52, 5783 (1970); D_o for NaCl and NaI taken from Ref. 24. Bond energies in the quenching gases taken from V.I. Vedeneyev, L.V. Gurvich, V.N. Kondrat'yev, V.A. Medvedev, and Ye. L. Frankevich, Bond Energies, Ionization Potentials, and Electron Affinities (St. Martin's Press, New York, 1966).

[b] For CH_3CN, from E.P. Lippincott, G. Nagarajan, and J.M. Stutman, J. Phys. Chem. 70, 78 (1966); for CF_3Cl, from W.N. Hess, R.L. Mather, and R.A. Nobles, J. Chem. Eng. Data 7, 317 (1962); all other values from Landolt-Bernstein Zahlenwerte und Functionen, A.M. Hellwege and K.H. Hellwege, Eds. (Springer-Verlag, Berlin), Vol. 1, Part 3 (1951), pp. 510ff.

FIGURE CAPTIONS

Fig. 1. Schematic sectional view (from the side) of the H_2 arc electrode arrangement, and a wiring diagram for DC operation. All distances are given in cm. and resistances in Ohms. The starting electrode is a ring of tantalum wire. The collimator is fabricated of molybdenum with a water-cooled copper sleeve and a large molybdenum disk to force the discharge to pass through the collimating orifice. The anode consist of a 2.5 cm diameter molybdenum disk mounted on a larger diameter ($\sim$5 cm) water-cooled copper disk. A 0.4 cm $\times$ 0.65 cm orifice is cut through the collimator and anode.

Fig. 2. The heavy solid curves (and dark circle data points) show the current through the arc as a function of DC voltage between the cathode and anode for various pressures of H_2 gas flowing through the arc housing. The lighter solid curves show contours of constant output intensity (measured in arbitrary units) at 2500 Å.

Fig. 3. The sodium D-lines reduced fluorescence (i.e., the ratio of the total number of D-lines photons detected per second to the number of ultraviolet photons per second incident on the NaI vapor) plotted, in arbitrary units, versus the nominal wavelength of the ultraviolet. Data points are given as solid symbols. The temperature at the bottom part of the NaI cell, where the solid NaI

resided, was 530°, 565°, and 603°C respectively for the data taken with vapor temperatures, at the cell window, of 633°, 664°, and 705°C. The bandwidths of the ultraviolet radiation were 24 Å (FWHM) for the 633°C vapor temperature experiment and 36 Å (FWHM) for the 664°C and 705°C experiments. The uncertainty in the ordinate for the data points increases rapidly as the wavelength is lowered below 2000 Å. The dashed lines show theoretical D-lines reduced fluorescence curves calculated for an NaI temperature of 633°C for transitions to the two upper repulsive potential curves shown in Fig. 4; the solid curve is the sum of the two dashed curves. All three sets of data points and the theoretical curve were normalized to unity at their long wavelength relative maximum.

Fig. 4. The repulsive potential curves for the two electronically excited states of NaI dissociating into $Na^*(3p) + I$ and $Na^*(3p) + I^*$ respectively and the NaI ground state potential curve which were used to fit the D-lines reduced fluorescence data of Fig. 3. Also shown are (1) the relative thermal populations at 633°C of the first ten vibrational levels of NaI, (2) unnormalized vibrational wave functions for the v = 0 and v = 9 levels of ground state NaI, and (3) three examples of continuum vibrational functions for the lower excited state of NaI. Note the break in the ordinate scale.

Fig. 5. Normalized probability density distributions for the LAB speed of an atom ejected with center-of-mass recoil energy given by Eq. (3) from a diatomic molecule with a thermal velocity distribution. The solid curves were calculated for the reduced speed A distribution considering only thermal translational energy in the target molecule, Eq. 17. The dashed curves were drawn for the reduced speed B probability density obtained by considering both thermal distributions in translational and rotational energies of the diatomic target; these reduced variable curves were calculated from Eq. (23) for the mass factors appropriate to the Na^* product of photodissociation of NaI. These second probability density functions are also given (unnormalized) in terms of the absolute Na^* speed for photodissociation of NaI at 1000°K.

Fig. 6. The lower panel shows the calculated normalized probability densities for speed of Na^* upon photodissociation of NaI by ultraviolet of the indicated wavelengths for a monochromator bandwidth function which is approximately triangular; the bandwidths quoted are the FWHM. Also shown as the bold solid curve is the Na^* speed distribution corresponding to a 906°K thermal distribution. The upper two panels show the normalized probability density functions for relative speed for collisions of the Na^* produced with the speed distributions given in the lowest panel with I_2 and C_2H_4 at 906°K. Also

shown, as bold solid curves, are the corresponding thermal distribution functions for relative speeds in the collisions.

Fig. 7. Upper Panel: The ratio of the reduced D-lines fluorescence for ethylene absent to that for ethylene present versus the ethylene pressure, for four ultraviolet wavelengths studied. The straight lines show the least squares linear fits of the primary data to the Stern-Volmer relation, Eq. (27). Lower Panel: The data points show plots of the phenomenological cross sections for collisional quenching of Na^* $(3p\,^2P)$ electronic excitation by ethylene, extracted from primary data such as is illustrated in the upper panel by means of Eq. (28), as a function of the characteristic relative collision speed given by Eq. (29). The error bars were obtained from the standard deviations of the slopes of the least squares linear fits of primary data to Eq. (27). The dash-dot-dash and dot-dot-dot curves show the true velocity dependence of cross sections $Q_q(g)$ assumed to vary as $K_5/g^{4/5}$ and $K_6/g^{2/3}$ respectively (with K_5 and K_6 given in Table I) which best fit the data. The solid and dashed curves show the corresponding fits to the data when these assumed functional forms of $Q_q(g)$ are averaged over the distribution in relative collision speeds.

Fig. 8. Cross sections for collisional quenching of Na^* by CO_2, C_6H_6, CF_3Cl, SO_2, and CH_3CN as a function of characterestic relative speed given by Eq. (29). The data points were evaluated by analyzing primary data by means of Eqs. (27) and (28); error bars reflect the standard deviations in k_q of least squares fits of primary data to Eq. (27). The curves show the best fits to the data points obtained by averaging cross section functions of the form $Q_q = K_s/g^{4/s}$ over the distribution in relative collision speeds: solid curve, s = 4; dashed curve, s = 5; dotted curve, s = 6. The values of K_s employed are listed in Table I.

Fig. 9. Upper Panel: Comparison of the velocity dependence of the $Na^* + I_2$ quenching cross sections reported in Ref. 11 (open squares) with the values arrived at in this work (open circles), if the data collected here is analyzed by the procedure employed in Ref. 11. Lower Panel: The velocity dependence of the $Na^* + I_2$ quenching cross section measured in this work. The temperature was 906°K. All conventions are as described for Fig. 8.

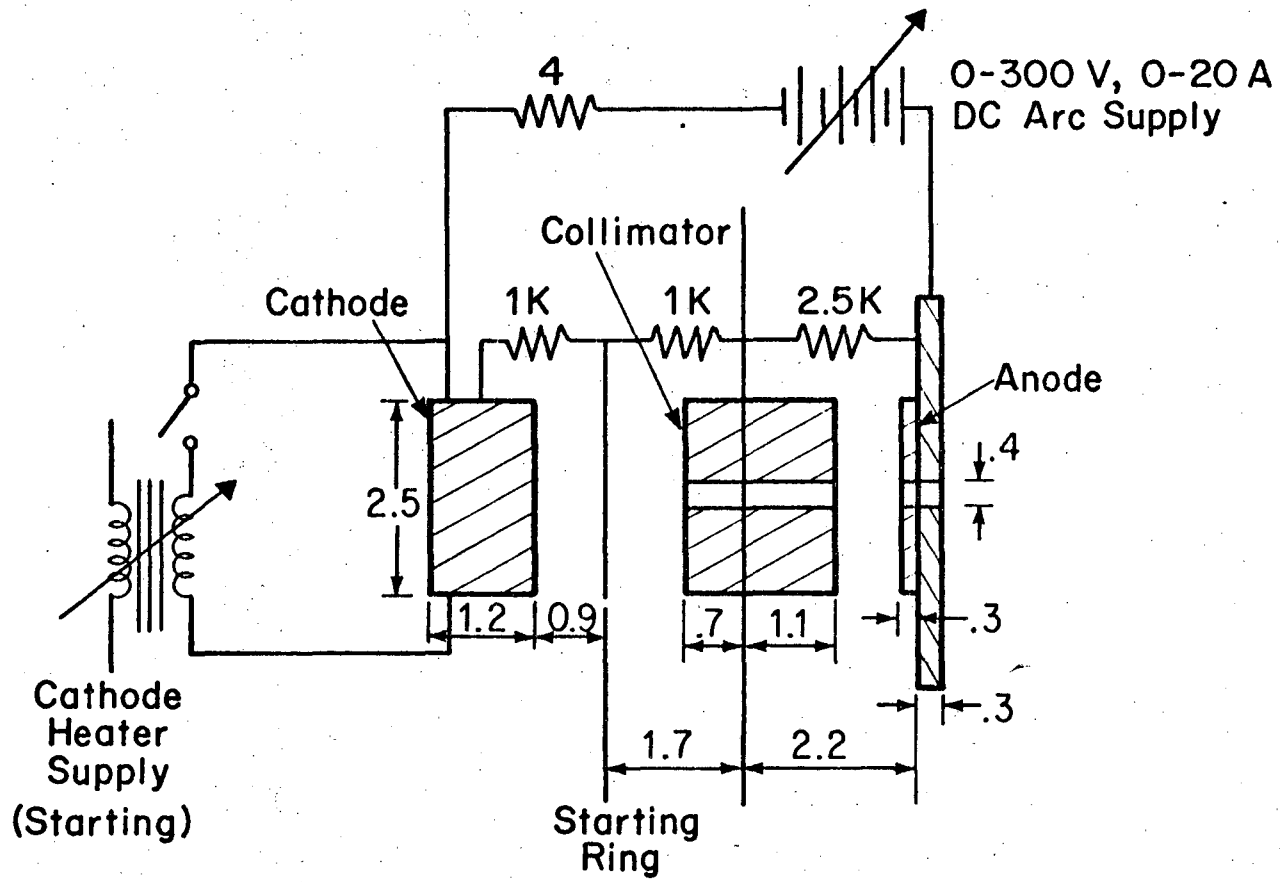

XBL 7012-7465

Fig. 1

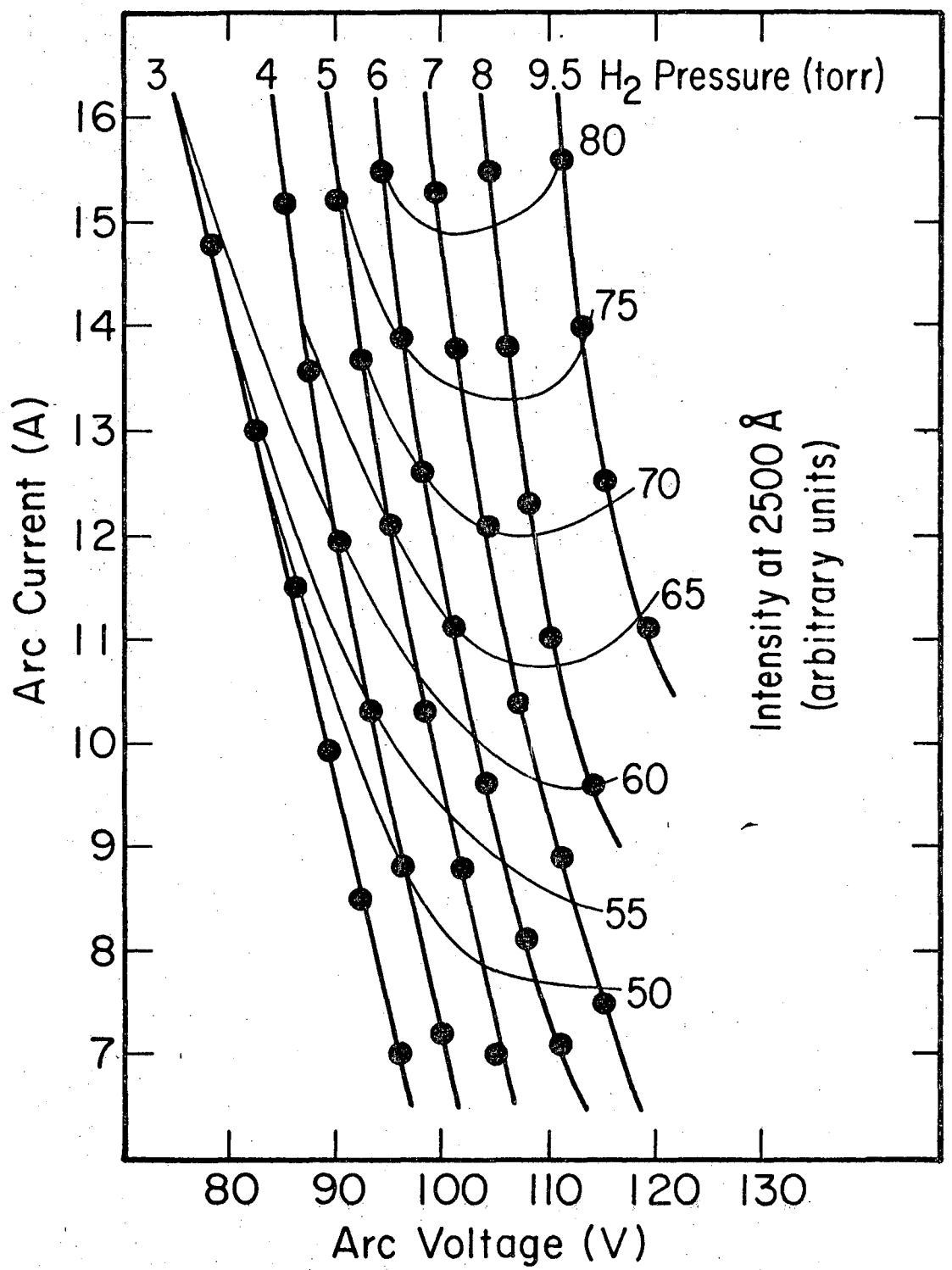

Fig. 2

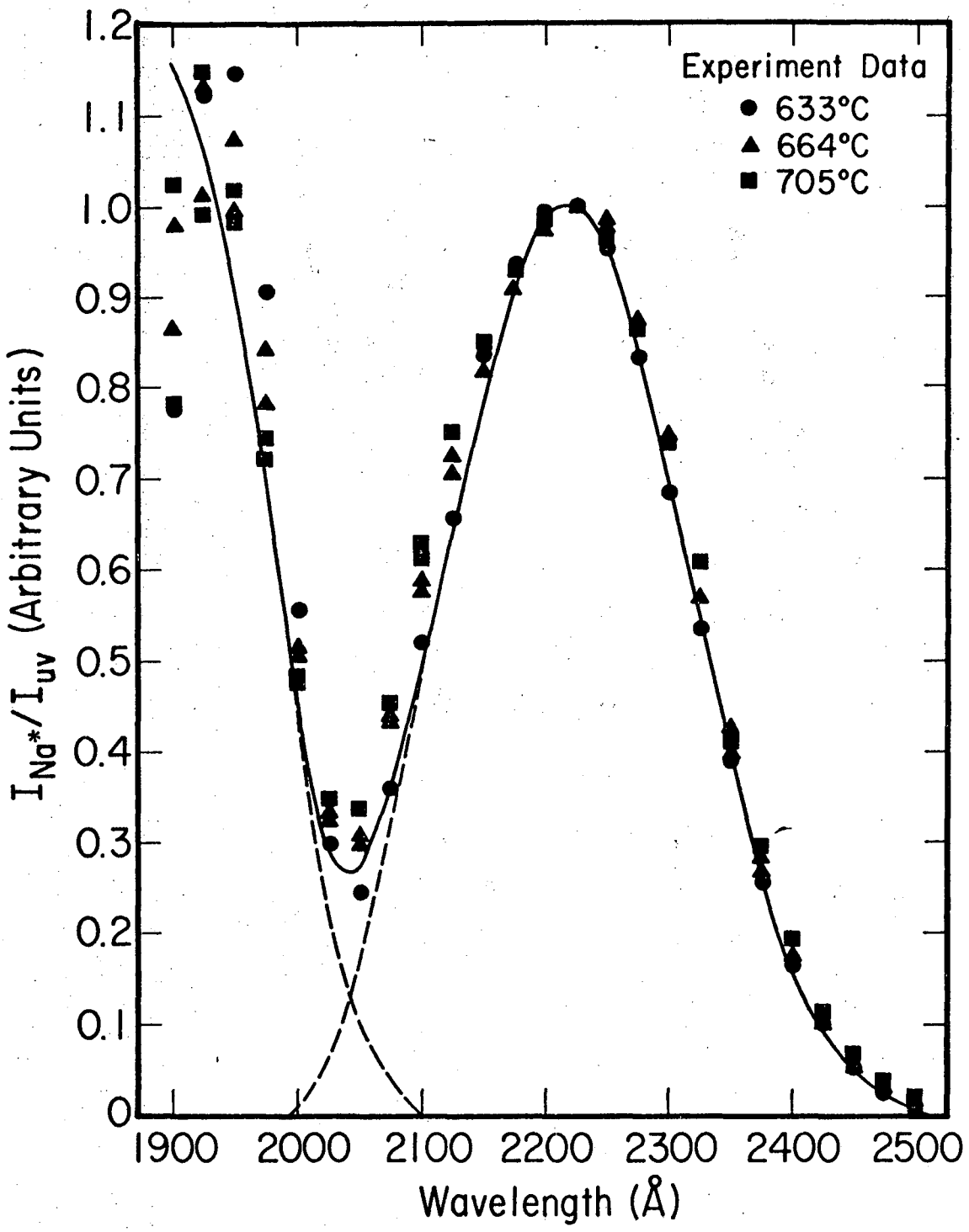
Experiment Data
633°C
664°C
705°C
I_{Na^*}/I_{uv} (Arbitrary Units)
Wavelength (Å)
1.2
1.1
1.0
0.9
0.8
0.7
0.6
0.5
0.4
0.3
0.2
0.1
0
1900
2000
2100
2200
2300
2400
2500
XBL 713-6601

Fig. 3

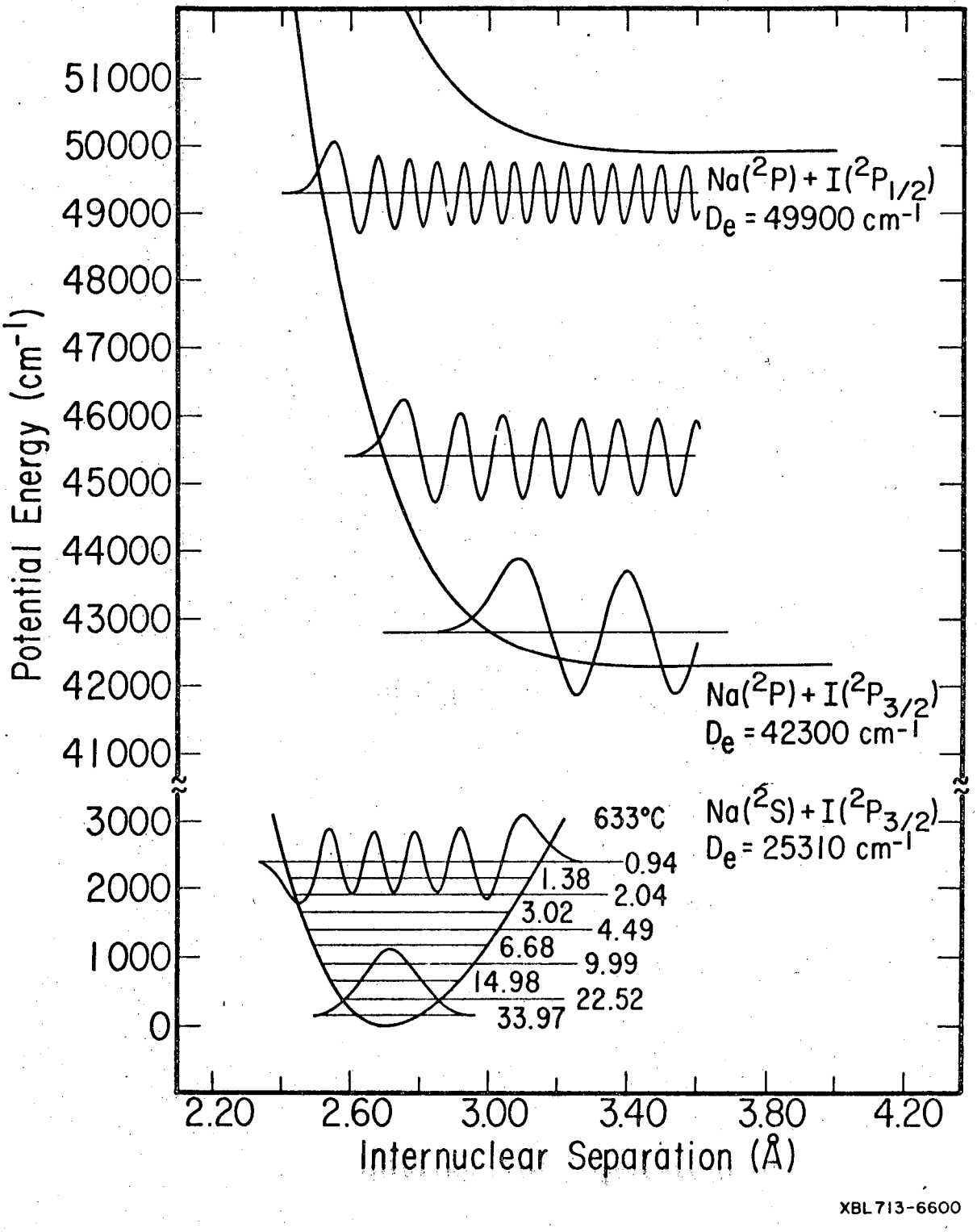

Fig. 4

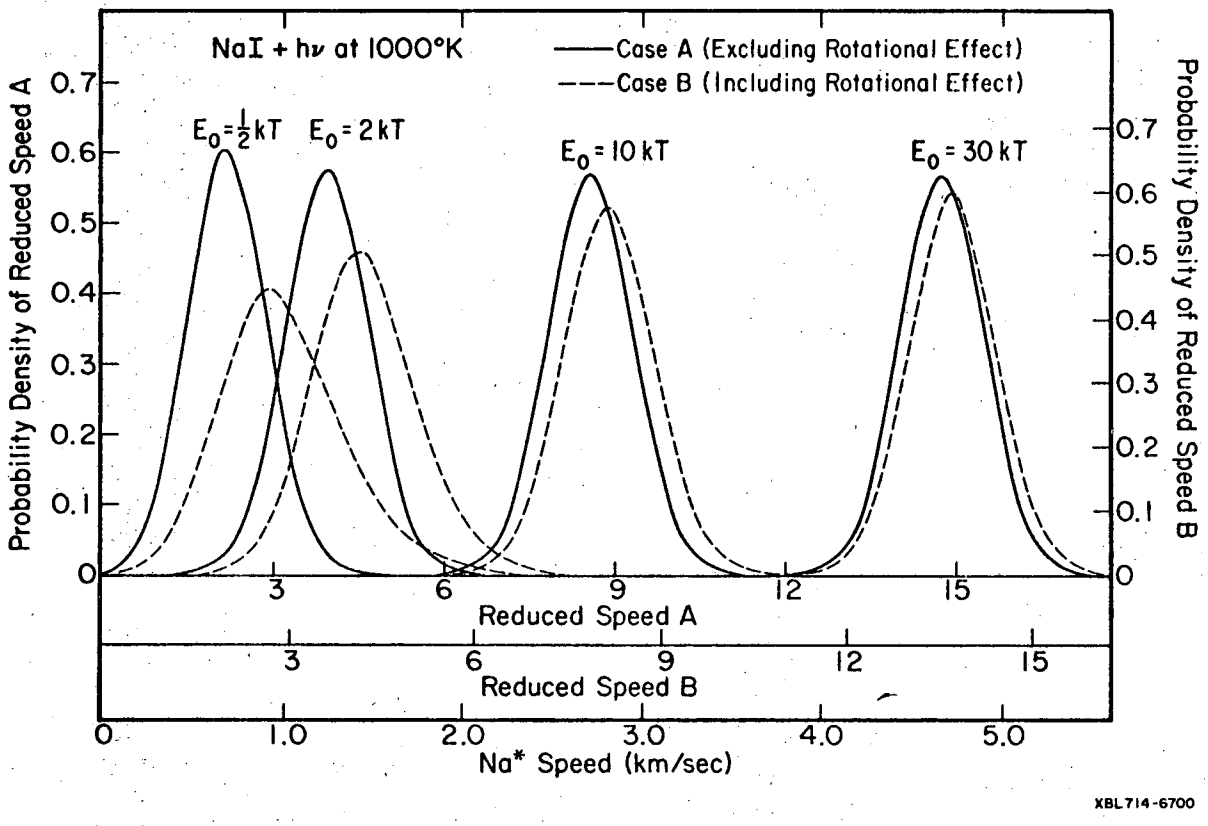
NaI + hν at 1000°K
Case A (Excluding Rotational Effect)
Case B (Including Rotational Effect)
$E_0 = \frac{1}{2}kT$
$E_0 = 2kT$
$E_0 = 10\,kT$
$E_0 = 30\,kT$
Probability Density of Reduced Speed A
Probability Density of Reduced Speed B
Reduced Speed A
Reduced Speed B
Na* Speed (km/sec)
XBL714-6700

Fig. 5

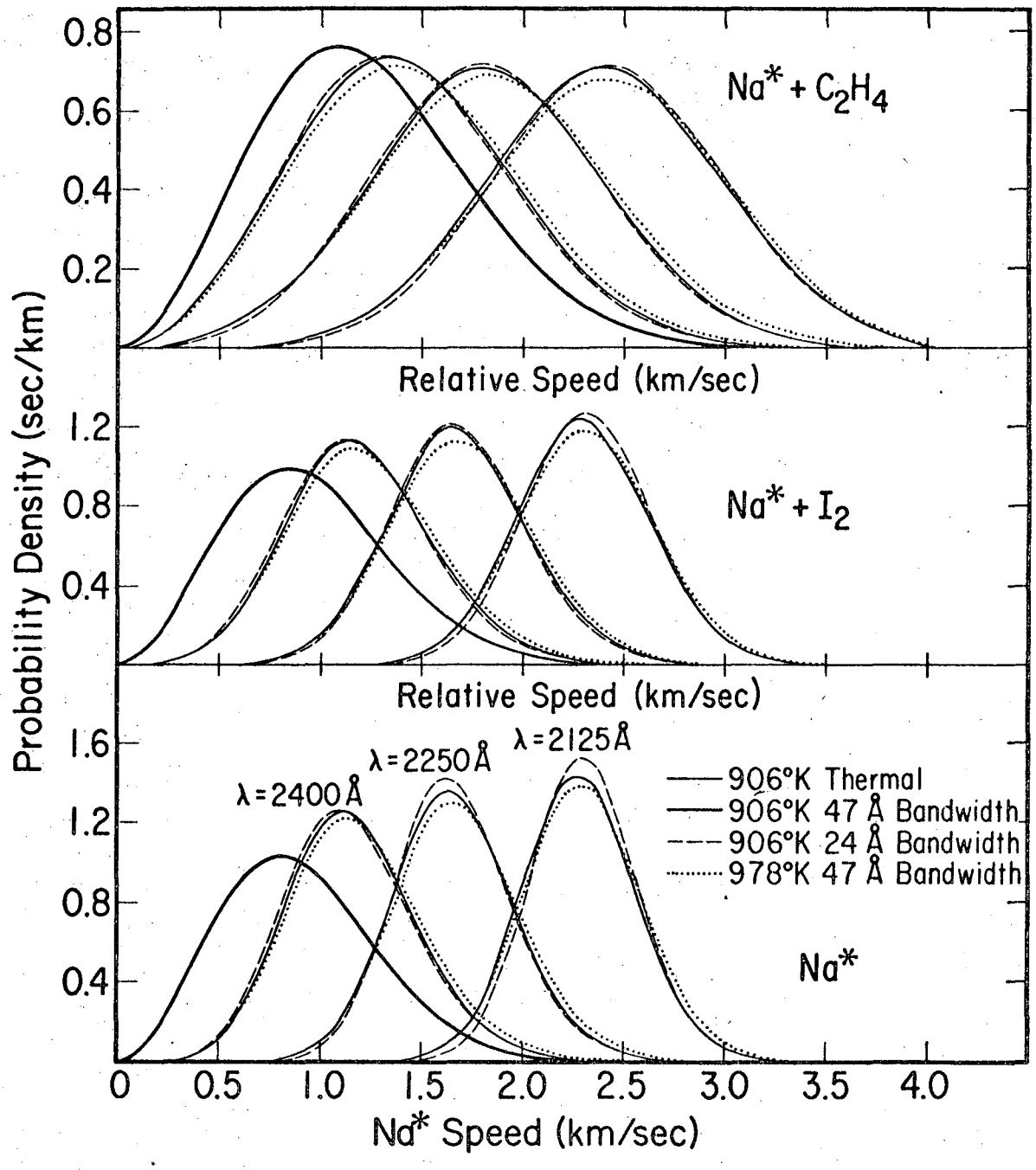

XBL 714-6673

Fig. 6

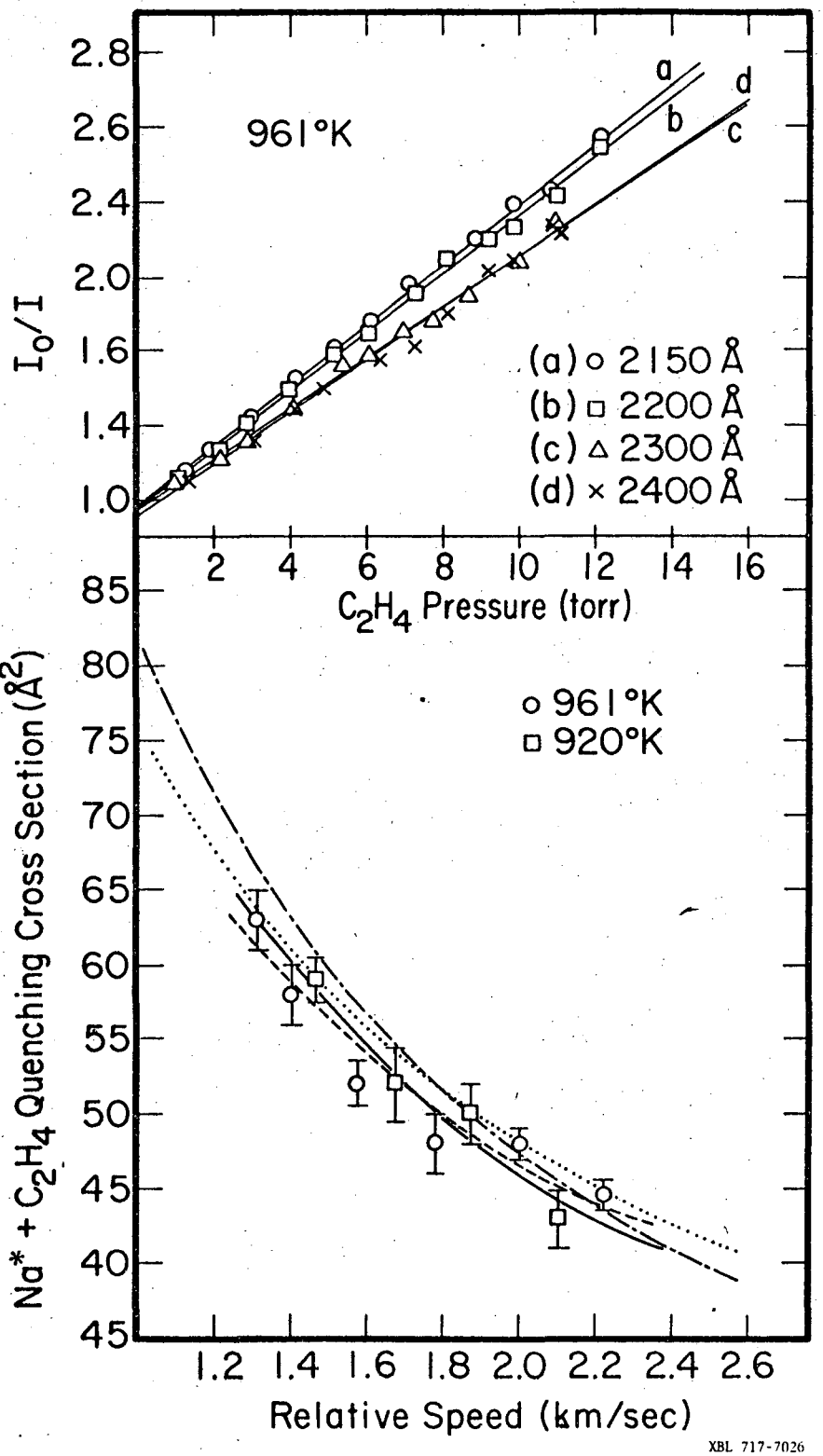
961°K
a
b
c
d
(a) ○ 2150 Å
(b) □ 2200 Å
(c) △ 2300 Å
(d) × 2400 Å
I_0/I
C_2H_4 Pressure (torr)
○ 961°K
□ 920°K
$Na^* + C_2H_4$ Quenching Cross Section ($Å^2$)
Relative Speed (km/sec)
XBL 717-7026

Fig. 7

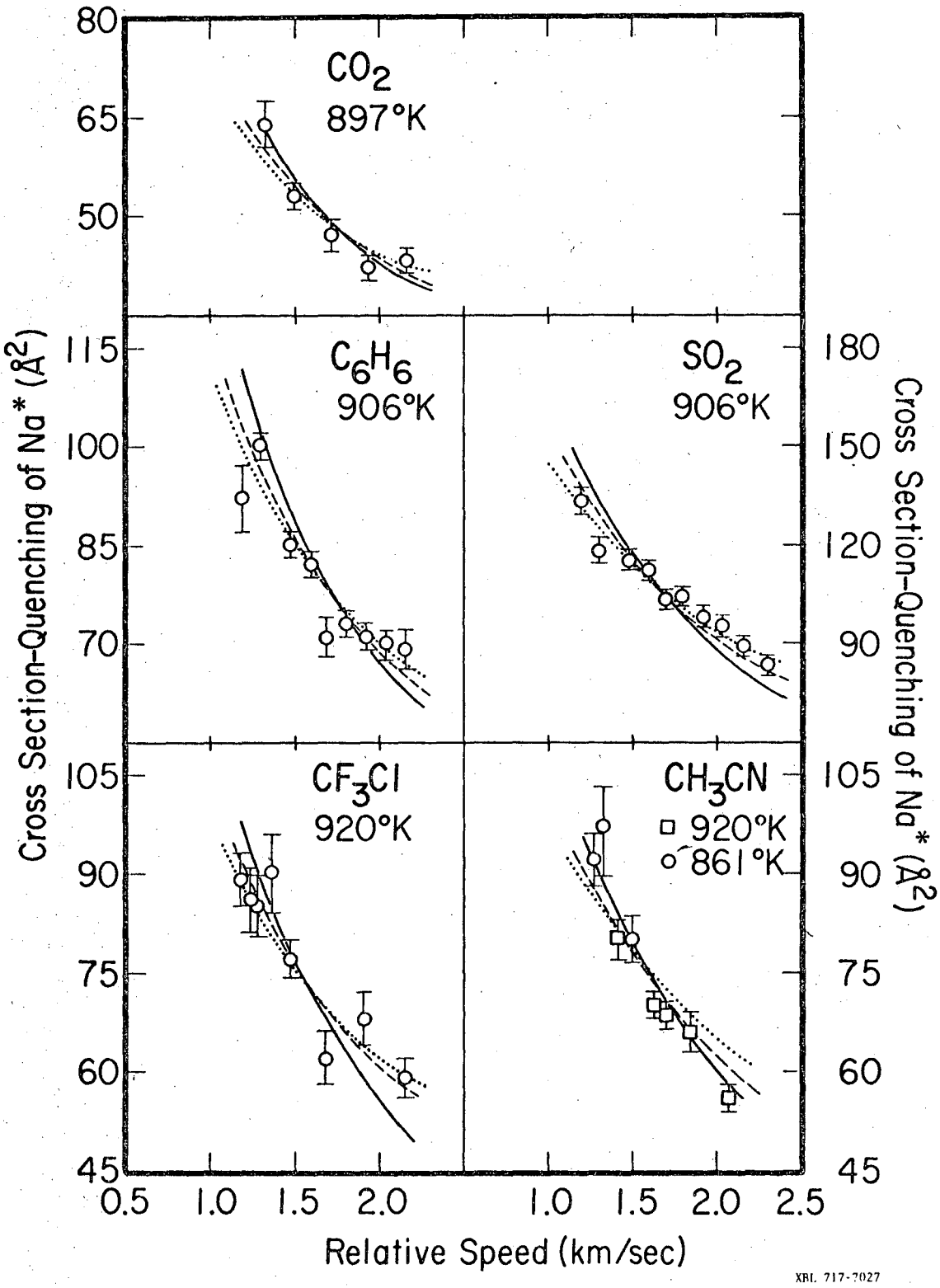
CO_2
897°K
C_6H_6
906°K
SO_2
906°K
CF_3Cl
920°K
CH_3CN
□ 920°K
○ 861°K
Cross Section-Quenching of Na* (Å²)
Relative Speed (km/sec)
XBL 717-7027

Fig. 8

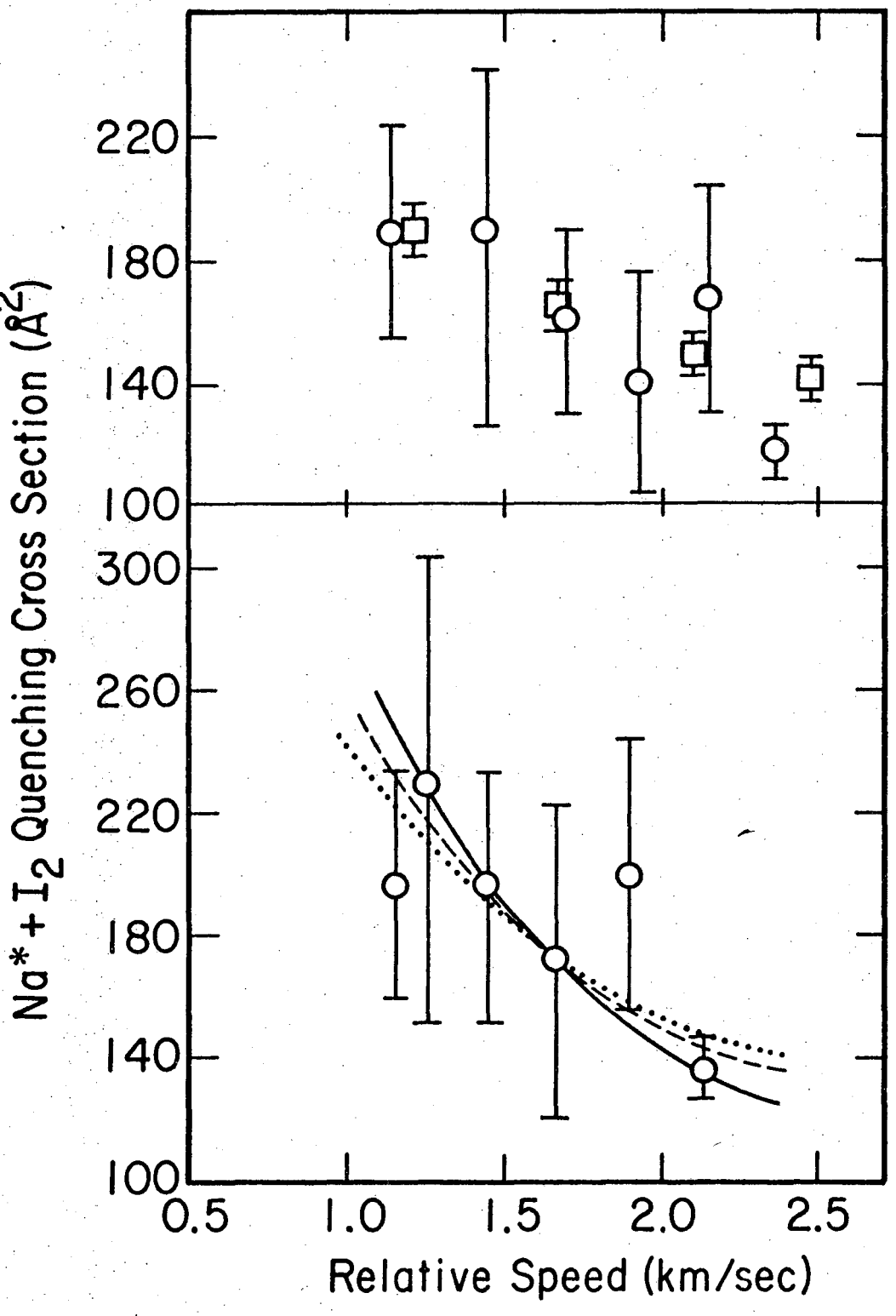
220
180
140
100
300
260
220
180
140
100
0.5
1.0
1.5
2.0
2.5
Na* + I2 Quenching Cross Section (Å2)
Relative Speed (km/sec)
XBL 717-7025

Fig. 9

TECHNICAL INFORMATION DIVISION
LAWRENCE BERKELEY LABORATORY
UNIVERSITY OF CALIFORNIA
BERKELEY, CALIFORNIA 94720